



U-Pb dating of chrysocolla from supergene copper deposits in the Coastal Cordillera of northern Chile, Atacama Desert

Juan Ríos-Contesse¹, Richard Albert^{2,3}, Benedikt Ritter-Prinz⁴, Axel Gerdes^{2,3}, Tibor Dunai⁴, Eduardo Campos¹

5 ¹Departamento de Ciencias Geológicas, Universidad Católica del Norte, Antofagasta, 1240000, Chile

2 Frankfurt Isotope and Element Research Center (FIERCE), Goethe University Frankfurt, Frankfurt, 60438, Germany

3 Department of Geosciences, Goethe University Frankfurt, Frankfurt, 60438, Germany

4 Institute of Geology and Mineralogy, University of Cologne, Cologne, 50674, Germany

10 *Correspondence to:* Juan Ríos-Contesse (juan.rios@ce.ucn.cl), Benedikt Ritter-Prinz (britter1@uni-koeln.de)

Abstract. The dating of supergene copper minerals has been widely used as a proxy to investigate the evolution and onset of hyperaridity in the Atacama Desert. However, investigation of supergene copper mineralisation in the Atacama Desert has been restricted to two physiographic units favourable for the industrial extraction of copper: the Central Depression and the Precordillera. Furthermore, these studies dated the timing of supergene mineralisation by secondary non-copper minerals like 15 alunite. In this study, we present new results of LA-ICP-MS U-Pb dating of chrysocolla from supergene deposits hosted in the western part of the Coastal Cordillera of northern Chile. The obtained U-Pb ages range from 8.4 ± 1.2 Ma to 0.046 ± 0.027 Ma. Supergene mineralisation ages point to significantly reduced precipitation, necessary for leaching and mineral precipitation process, since the Late Miocene to Pleistocene in the Coastal Cordillera, later than the secondary supergene mineralisation ages from the Precordillera. ~~Post Mid-to-Late Miocene ages~~ point to repeated phases of sufficient moisture along the Coastal Cordillera that ~~promotes~~ chrysocolla mineralisation during the Pliocene and Pleistocene. We propose that 20 due to the position of the study areas near the coastal escarpment, and the predominant hyperarid environment in this part of the Coastal Cordillera since at least the Mid-Miocene, pluvial periods and/or intensification of coastal fog events caused alternating phases of supergene activity.

1 Introduction

25 The evolution and onset of hyperaridity in the Atacama Desert is a subject of ongoing debate. The hypothesis that the onset of hyperaridity occurred during the Oligocene-Miocene transition has been postulated by some authors (e.g. Dunai et al., 2005; Evenstar et al., 2009; Ritter et al., 2018a). In contrast, other authors have proposed the Middle Miocene period (e.g. Sillitoe and McKee, 1996; Jordan et al., 2014; Evenstar et al., 2017). Furthermore, it has been suggested that the Middle-Late Miocene period may be more appropriate (Rech et al., 2010), while others have proposed the Pliocene (Hartley and Chong, 30 2002; Hartley and Rice, 2005; Sáez et al., 2012; Oerter et al., 2016). Also, the Pleistocene has ~~also~~ been proposed by some authors (Placzek et al., 2010; Amundson et al., 2012). The variability in ages and interpretations is mainly related to the regional distribution of evidence, the sensitivity of the proxies used and the local climate gradients (Ritter et al., 2018a) (Fig.



1). The proxies that have been used to determine the onset of hyperaridity in the Atacama Desert can be separated in three groups (Fig. 1): 1) Supergene minerals: implies the dating by the K-Ar and Ar-Ar methods of minerals that were formed by 35 supergene processes such as alunite group minerals and Mn-oxides (Gustafson and Hunt, 1975; Alpers and Brimhall, 1988; Sillitoe and McKee, 1996; Marsh et al., 1997; Mote et al., 2001; Bouzari and Clark, 2002; Arancibia et al., 2006; Warr 2008; Bissig and Riquelme, 2010; Perelló et al., 2010; Hervé et al., 2012; Riquelme et al., 2018). Also, gypsum and pseudomalachite have been dated by Th-U and U-Pb methods respectively (Reich et al., 2009; Kahou et al., 2021); 2) Sedimentological studies: include the interpretation of stratigraphic records and the determination of erosion rates (Hartley 40 and Chong, 2002; Wörner et al., 2002; Amundson et al., 2012; Sáez et al., 2012; Jordan et al., 2014; Placzek et al., 2014); and 3) Surfaces studies: based on the determination of surface exposure ages, stable isotopes composition in carbonates and the characterisation of paleosols (Dunai et al., 2005; Evenstar et al., 2009; 2017; Placzek et al., 2010; Rech et al., 2010; Oerter et al., 2016; Ritter et al., 2018a; 2018b; Muñoz-Fariás et al., 2023).

The supergene copper minerals are produced by the interaction between hypogene sulphide mineralisation, tectonic uplift, 45 host rock composition and water availability (Chávez, 2000; Hartley and Rice, 2005; Shaw et al., 2021). The precipitation rate required to develop supergene mineralisation is estimated to be above 120 mm mean annual rainfall (MAR) (Evenstar et al., 2024). The reaction between meteoric waters and sulphides such as pyrite, cause the acidification of infiltrating and percolating waters that will enhance the leaching potential of Cu-bearing sulphides (e.g. chalcopyrite and bornite) and 50 remobilise copper in or above the water table, where environmental conditions are oxidative. The upper part of a typical supergene profile contains abundant Fe-bearing minerals such as hematite or jarosite that may be mixed with Cu-bearing minerals (e.g. atacamite, chrysocolla and brochantite). The youngest age of supergene mineralisation is interpreted as the last time with sufficient moisture to activate the process (Hartley and Rice, 2005); therefore, it will reflect the transition from arid conditions (100-300 mm MAR) towards hyperarid conditions (<100 mm MAR) (Alpers and Brimhall, 1988; FAO, 55 Sillitoe and McKee, 1996).

55 Previous studies propose that the supergene processes across the entire Atacama Desert were active from Eocene to Late Pleistocene (Hartley and Rice, 2005; Arancibia et al., 2006; Reich et al., 2009; Evenstar et al., 2024). Dating of supergene minerals in the Atacama Desert were obtained mainly from supergene alunite mineral group (alunite, jarosite, natroalunite and natrojarosite) by the K-Ar and Ar-Ar dating methods and were focused mainly on deposits hosted in the Precordillera and the Central Depression (Gustafson and Hunt, 1975; Alpers and Brimhall, 1988; Sillitoe and McKee, 1996; Marsh et al., 60 1997; Mote et al., 2001; Bouzari and Clark, 2002; Arancibia et al., 2006; Bissig and Riquelme, 2010; Riquelme et al., 2018), except for one age reported in the Coastal Cordillera by Sillitoe and McKee (1996) (Fig. 1). Although the supergene alunite mineral group can be found near or intergrown with supergene copper minerals, their synchronous precipitation is not always ensured (Kahou et al., 2021). Therefore, the obtained ages in these supergene minerals might be biased by differential dissolution and reprecipitation processes and not be accurate to constrain the age of supergene copper mineralisation (Kahou 65 et al., 2021). Mn-oxides such as cryptomelane and birnessite have been successfully dated using the K-Ar and Ar-Ar methods (Mote et al., 2001; Arancibia et al., 2006; Riquelme et al., 2018). These minerals can co-precipitate with



chrysocolla forming copper pitch/copper wad (Dold et al 2023); therefore, the yielded ages can be directly related to the precipitation of supergene copper mineralisation. Furthermore, some studies have successfully dated supergene copper-bearing minerals such as atacamite, yielding ages between 236.6 ± 8.0 and 75.3 ± 0.4 ka (using Th-U method), the latter being the youngest age obtained in a supergene profile in the Atacama Desert (Reich et al., 2008; 2009). Three of those ages were obtained in the Coastal Cordillera (Fig. 1). Finally, Kahou et al. (2021) reported an age of 18.4 ± 1.0 Ma in pseudomalachite (using U-Pb method) which is interpreted as the formation age of the Mina Sur exotic-type copper deposit. The present study focuses on the dating of chrysocolla hosted in copper deposits from the Coastal Cordillera because: 1) the supergene mineralisation of chrysocolla requires meteoric water sourced from precipitation events or episodes, making it a potential new proxy to better understand the palaeoclimatic evolution of the Coastal Cordillera; 2) chrysocolla is the most abundant supergene mineral in the Coastal Cordillera; 3) until now, no other supergene mineral phase that can be dated such as alunite or goethite has been found in deposits within the Coastal Cordillera; and 4) the Coastal Cordillera of Atacama Desert remains largely unexplored for supergene deposits, mainly due to their low economic value compared to the copper deposits found in the Precordillera.

80 2 Geological setting

The Coastal Cordillera is the westernmost morphotectonic unit in northern Chile (Fig. 1). It forms a prominent topographic feature that is more than 1000 km long and 20-50 km wide, with an average altitude of 1500 m a.s.l. reaching a maximum of 3100 m a.s.l. (Hartley et al., 2005; Quezada et al., 2010). It corresponds to a Jurassic-Early Cretaceous magmatic arc (Scheuber et al., 1994; Scheuber and González, 1999) created during the first stages of the Andean cycle (Coira et al., 1982; Charrier et al., 2009). The magmatic arc corresponds to a volcanic sequence named La Negra Formation (García, 1967), which is mainly made up of andesites and basaltic andesites intruded by numerous plutonic bodies of different sizes and compositions that vary from gabbros to tonalites (Charrier et al., 2007; Oliveros et al., 2020).

The Coastal Cordillera hosts the largest number of mineral deposits in the Antofagasta Region, the majority of which are copper deposits (Boric et al., 1990) (Fig. 2). Within the Coastal Cordillera, an eastern metallogenic belt is characterised by Early Cretaceous breccia-style hydrothermal mineralisation and porphyry copper deposits (Perelló et al., 2003; Palacios et al., 2007). On the other hand, there is a western metallogenic belt consisting of Late Jurassic stratabound (also known as manto-type) and vein-type copper deposits formed between 170 and 155 Ma (Boric et al., 1990; Maksaev et al., 2006; Tristá-Aguilera et al., 2006; Palacios et al., 2007). The manto-type deposits are hosted in lavas of the La Negra Formation, whereas the vein-type are emplaced in intrusive rocks (Tristá and Kojima, 2003). Both deposit types are epigenetic and are formed by the interaction between magmatic fluids from cooling intrusions with a moderate contribution of fluids leached from the volcanic host rocks (Barra et al., 2017).

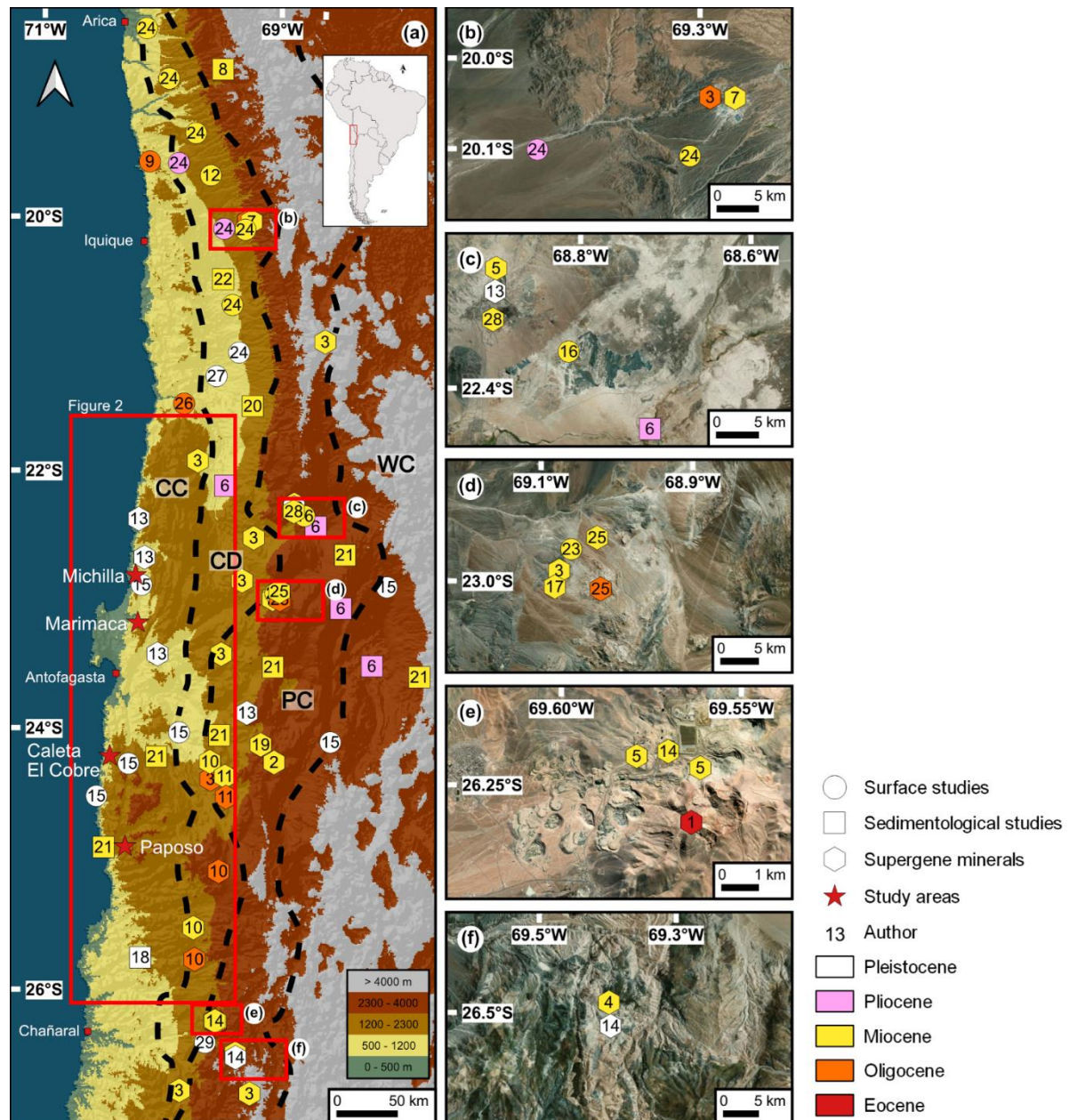


Figure 1. (a) Colour shaded digital elevation model (derived from GMTED2010-data, created using QGIS 3.20.3-Odense). Compilation of dates archives for the proposed various onsets of hyperaridity in the Atacama Desert. Colours define the time: red: Eocene; orange: Oligocene; yellow: Miocene; pink: Pliocene; white: Pleistocene. Shapes define the study: hexagon: supergene minerals; square: sedimentological studies; circle: surface studies. Physiographic units: CC: Coastal Cordillera; CD: Central Depression; PC: Precordillera; WC: Western Cordillera. **1:** Gustafson and Hunt 1975; **2:** Alpers and Brimhall 1988; **3:** Sillitoe and McKee 1996; **4:** Marsh et al., 1997; **5:** Mote et al., 2001; **6:** Hartley and Chong 2002; **7:** Bouzari and Clark 2002; **8:** Wömer et al., 2002; **9:** Dunai et al., 2005; **10:** Arancibia et al., 2006; **11:** Warren et al., 2008; **12:** Evenstar et al., 2009; **13:** Reich et al., 2009; **14:** Bissig and Riquelme 2010; **15:** Placzek et al., 2010; **16:** Rech et al., 2010; **17:** Perelló et al., 2010; **18:** Amundson et al., 2012; **19:** Hervé et al., 2012; **20:** Sáez et al., 2012; **21:** Placzek et al., 2014; **22:** Jordan et al., 2014; **23:** Oerter et al., 2016; **24:** Evenstar et al., 2017; **25:** Riquelme et al., 2018; **26:** Ritter et al., 2018a; **27:** Ritter et al., 2018b **28:** Kahou et al., 2021; **29:** Muñoz-Farías et al., 2023.



The copper-bearing minerals in the deposits hosted in the western belt usually occur as dissemination in the host rock, amygdale-filling, stockworks, thin veinlets and crusts (Sato, 1984; Kojima et al., 2003; 2009). The copper-bearing minerals
110 can be grouped into three different types of mineralisation: (1) The hypogene mineralisation type is characterised by copper sulphides such as chalcocite, digenite, bornite and minor chalcopyrite with iron oxide mainly magnetite and hematite
Kojima et al., 2003; 2009).

This type of mineralisation has been dated between 170 and 155 Ma. (Maksaev et al., 2006; Tristá-Aguilera et al., 2006) and
115 is associated with a hydrothermal alteration characterised by albite, epidote, calcite, chlorite, sericite, actinolite and quartz
mineralisation (Vivallo and Henríquez, 1998; Kojima et al., 2009). (2) The supergene sulphide mineralisation type consists
of fine-grained aggregates of supergene chalcocite and covellite (Boric et al., 1990; Kojima et al., 2003). This type of
mineralisation is poorly developed and is not observed in all deposits (Boric et al., 1990; Maksaev and Zentilli, 2002). (3)
Finally, the oxide mineralisation type is characterised by chrysocolla and atacamite as the main mineral phases with minor
copper pitch/copper wad, malachite and chenevixite (Boric et al., 1990; Maksaev and Zentilli, 2002; Kojima et al., 2003;
120 Mateo et al., 2023).

Chrysocolla is an amorphous hydrated copper silicate (Frost and Xi, 2013) with the following chemical formula
 $Cu_{2-x}Al_x(H_{2-x}Si_2O_5)(OH)_4 \cdot nH_2O$ ($x < 1$, $n \sim 0.25$) (Torpy et al., 2021; Dold et al., 2023) that precipitates from gel-like material
(Newberg, 1967; Moreton, 2007; Hariu et al., 2013). Its formation is restricted to a pH between 5 and 9 and a high
125 concentration of silica (Newberg, 1967; Yates et al., 1998; Dold, 2006; De Putter et al., 2010). Furthermore, chrysocolla may
occur as a replacement for other copper minerals such as malachite and atacamite (Crane et al., 2001; Sillitoe, 2005). On the
sites selected for this study chrysocolla occurs abundantly as a supergene mineral related to the manto- and vein-type
hypogene copper deposits (Boric et al., 1990; Kojima et al., 2003; Tristá and Kojima, 2003).

3 Material and methods

3.1 Sampling strategy

130 The sampling of chrysocolla was carried out in four selected sites, all located close to the coastal cliff on the western
metallogenic belt of the Coastal Cordillera: Michilla area (MI), Marimaca area (MA), Caleta El Cobre area (CC) and Paposo
area (PA) (Fig. 2). The sites were selected considering the access to mining excavations located at different heights (from
nearly 2,000 m a.s.l. to less than 500 m a.s.l.). A total of 154 samples were taken in-situ from mining excavations within the
135 four study areas (Fig. 2) and chips of each sample were mounted in epoxy resin mounts ($\varnothing 24$ mm) and polished at the
Universidad Católica del Norte, Chile.



3.2 Micro-X-ray fluorescence (μ XRF)

μ XRF geochemical maps for this study were produced on a Bruker Tornado M4 μ XRF two detector system at the Institute for Geography of the University of Cologne (UoC), Germany. The mapping was performed under vacuum conditions using a 20 μ m step size and 20 μ m spot size at 15 ms per pixel, two frame counts and 50 kV acceleration.

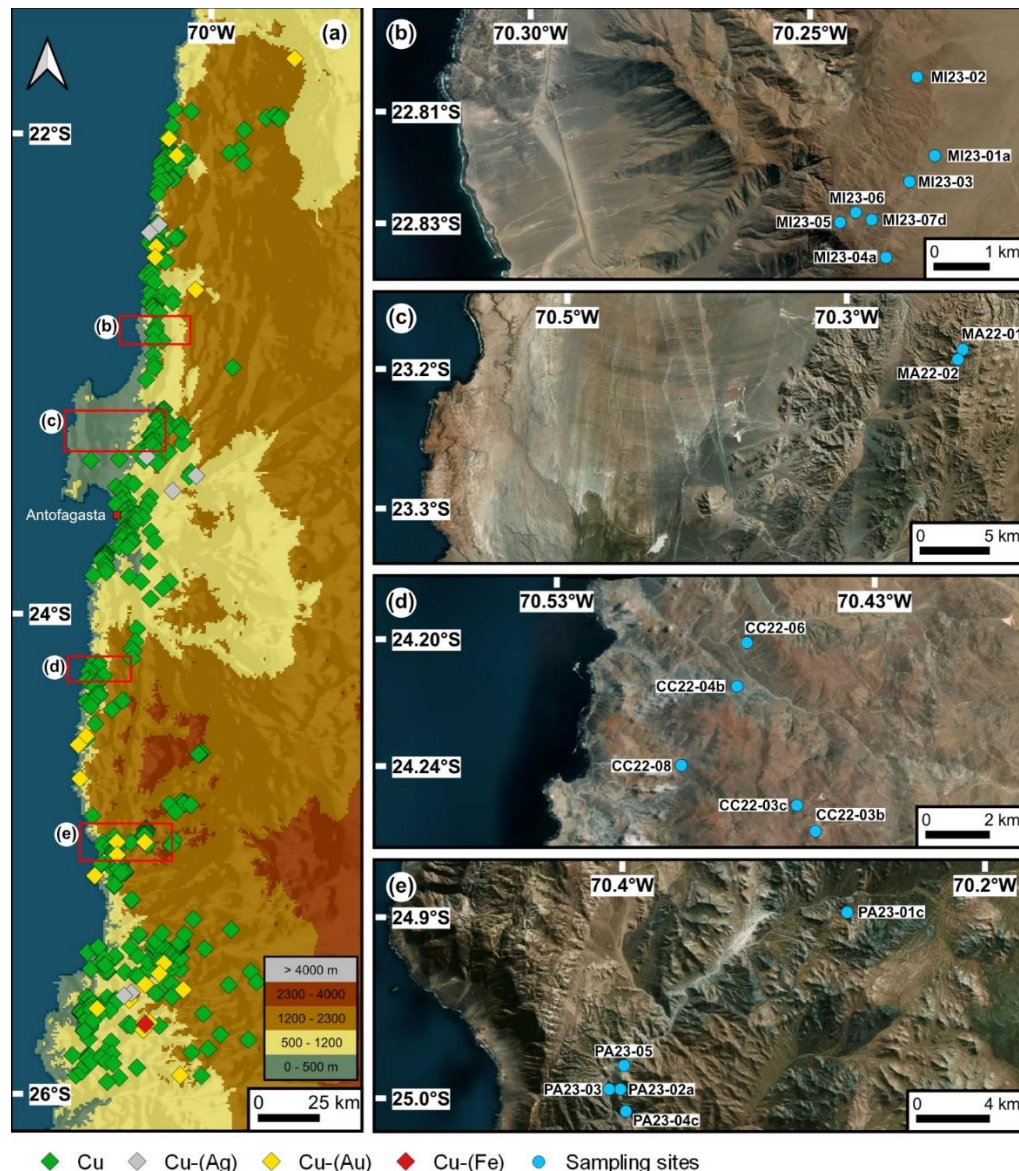


Figure 2. (a) Colour shaded digital elevation model (derived from GMTED2010-data, created using QGIS 3.20.3-Odense). (a) Map with copper mineral deposits hosted in the Coastal Cordillera. Data taken from Boric et al. (1990). (b-e) Maps of the study areas showing selected sampling sites (b) Michilla area; (c) Marimaca area; (d) Caleta El Cobre area; (e) Paposo area. For all the sampling sites see Supplementary File 1.



145 3.3 Raman spectroscopy

Raman spectra were obtained with a Renishaw InVia Qontor Raman microscope at the Institute for Geology and Mineralogy, UoC, Germany. Spectrometer calibration was performed before analysis with a built-in silicon standard. Raman spectra of the polished samples were obtained after manually focusing the 532 nm Ne: YAG laser (100 mW) with a x10 objective (NA = 0.25) on the sample surface. A Centrus 1AY701 front-illuminated CCD detector was used in combination 150 with an 1800 lines mm⁻¹ grating and a slit opening of 65 µm. The estimated resolution is about 2.3 cm⁻¹. Spectra were recorded continuously from 100 to 4000 cm⁻¹ in the SynchroScan™ mode for 10 accumulations with an individual exposure time of 10 seconds. Mineral identification was performed by comparison with the RRUFF database (Lafuente et al., 2016). We used µXRF and Raman spectroscopy to enhance the analytical identification of minerals identified in our sample set.

3.4 U-Pb LA-ICP-MS dating

155 In-situ U-Pb dating was carried out using laser ablation-inductively coupled plasma mass spectrometry (LA-ICPMS) at FIERCE (Frankfurt Isotope and Element Research Centre, Goethe University Frankfurt). A ThermoScientific ElementXr sector field ICPMS was coupled to a RESolution 193 nm ArF excimer laser (COMplexPro 102) equipped with a two-volume ablation cell (Laurin Technic S155).

Data were acquired in fully automated mode overnight during three analytical sessions. Analytical parameters can be found 160 in Supplementary dataset. Raw data were corrected using an in-house VBA spreadsheet program (Gerdes and Zeh, 2006; 2009). No common-Pb correction was applied to the data.

To our knowledge, no chrysocolla reference material (RM) exists. Therefore, the standardisation strategy used to control the reproducibility and accuracy of the chrysocolla analyses was the following. NIST SRM612 reference glass was used as a primary RM to correct for instrumental mass bias, concentration calculations and to tune the instruments. To account for the 165 matrix related bias on the $^{238}\text{U}/^{206}\text{Pb}$ ratios of chrysocolla we used another three RM of different and contrasting compositions, *i.e.*: zircon, monazite and titanite. We added to the uncertainty budget of each of the analytical sessions, an excess of scatter so that the weighted average of the $^{238}\text{U}/^{206}\text{Pb}$ and $^{207}\text{Pb}/^{206}\text{Pb}$ ratios of each of the secondary RM had an MSWD ≤ 1 . We also calculated the range of dispersion of the $^{238}\text{U}/^{206}\text{Pb}$ ratios between the four RM and added this bias quadratically as a systematic uncertainty on all calculated dates. An assumed 4% (2s) as a long-term reproducibility value 170 was also added.

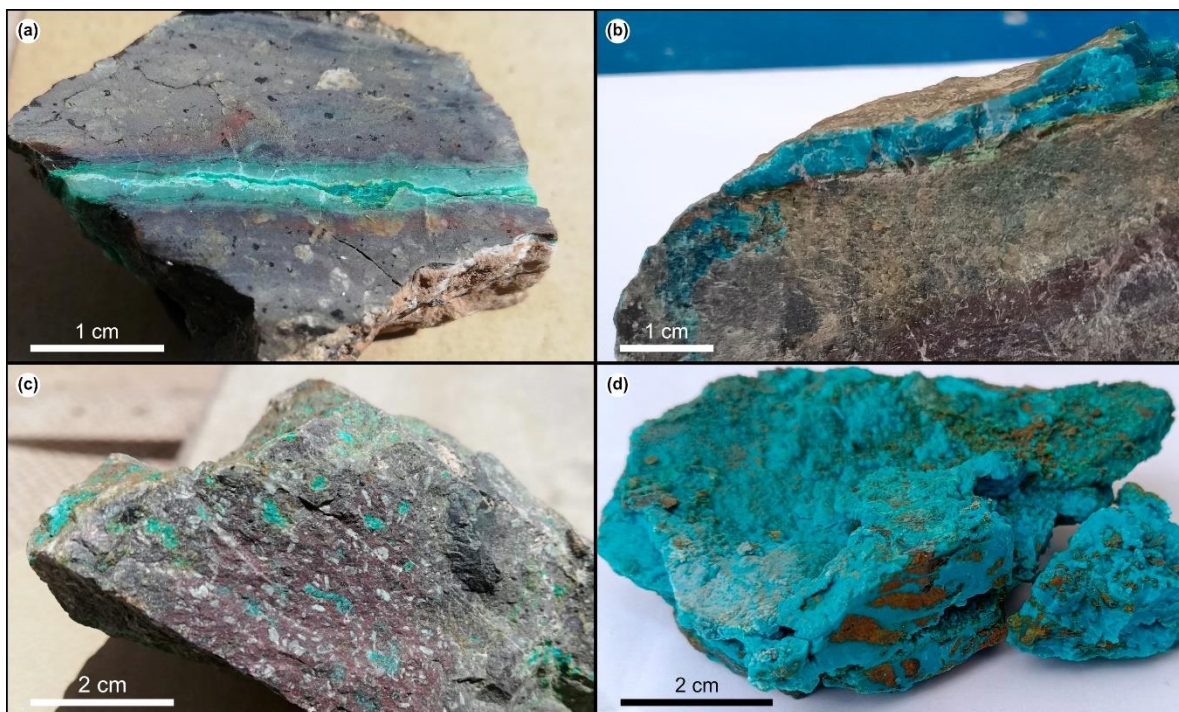
We established a pre-screening strategy to target suitable samples, due to potential high initial Pb to radiogenic Pb concentrations in chrysocolla. Therefore, 66 mounts were prepared and pre-screened to enhance the success dating rate. This pre-scan method consists of quickly ablating different areas of the samples, while monitoring the $^{238}\text{U}/^{206}\text{Pb}$ and $^{207}\text{Pb}/^{206}\text{Pb}$ ratios, to determine which areas were prone to contain suitable and favourable ratios. After scanning the sample, if 175 appropriate areas were found, the laser spots were placed for further analysis.



4 Results

4.1 Petrographic observations

In the study areas chrysocolla can be found filling cracks in the host rock, as millimetre crusts covering the host rock, or filling amygdales within andesite (Fig. 3a-c). Also, it is possible to find it massive, but it is less common (Fig. 3d). Under the 180 optical microscope, it is common to find banding and botryoidal texture in the chrysocolla (Fig. 4a-b). The banding texture is a consequence of physicochemical changes in the ore-forming fluids and the environment of mineralisation over time (Craig and Vaughan, 1981). Occasionally, chrysocolla can appear partially replacing malachite (Fig. 4c-d). The chrysocolla exhibits a replacement textural relationship with atacamite, the second most abundant mineral in our samples. In hand specimens, atacamite is observed as a thin crust covering the chrysocolla (Fig. 5a-b). Microscopically, chrysocolla is cut by atacamite 185 (Fig. 5c-d). Additional minerals identified in hand specimens include diopside and copper pitch, gypsum, goethite, quartz, epidote and zeolite. Furthermore, sulphides such as pyrite, chalcopyrite, bornite, chalcocite and covellite are observed in some samples.



190 **Figure 3.** Macroscopic textures of chrysocolla in the study areas. (a) Veins that form by filling cracks on the host rock in sample MI7-6. (b) Millimetre crust covering the host rock in sample CC22-03-10. (c) Filling amygdales on the andesites of La Negra Formation in sample CC2-12. (d) Massive, the less common of the textures in sample CC22-06-02.

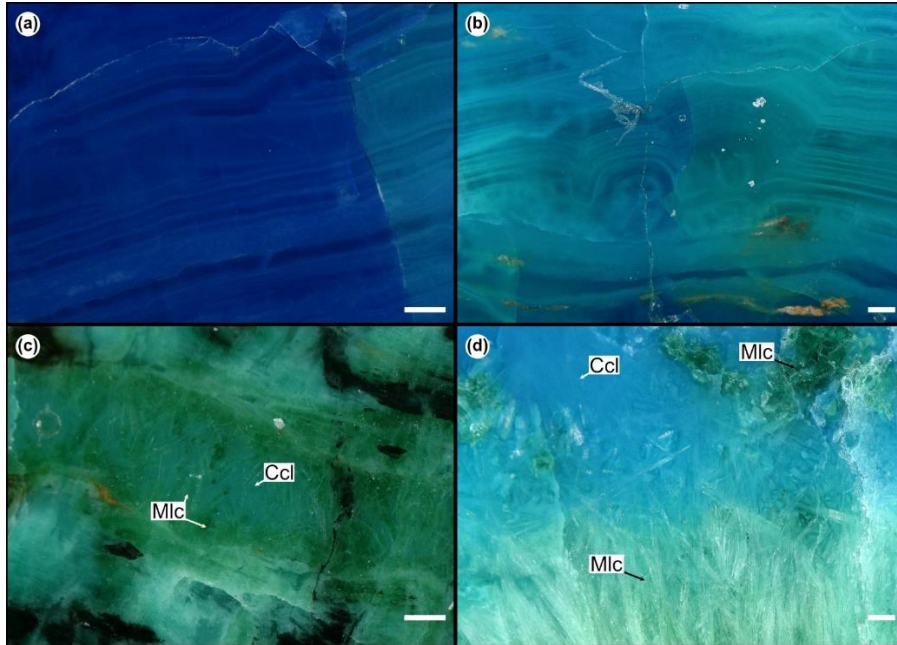


Figure 4. Photomicrograph of chrysocolla textures. **(a)** Banding in chrysocolla in sample MI23-03-03. **(b)** Botryoidal texture and banding in chrysocolla in sample CC22-03-10. **(c-d)** Replacement of malachite with chrysocolla: **(c)** sample CC2-6, **(d)** sample MI23-04-05. **Ccl:** chrysocolla, **Mlc:** malachite. All scale bars are 100 µm.

195

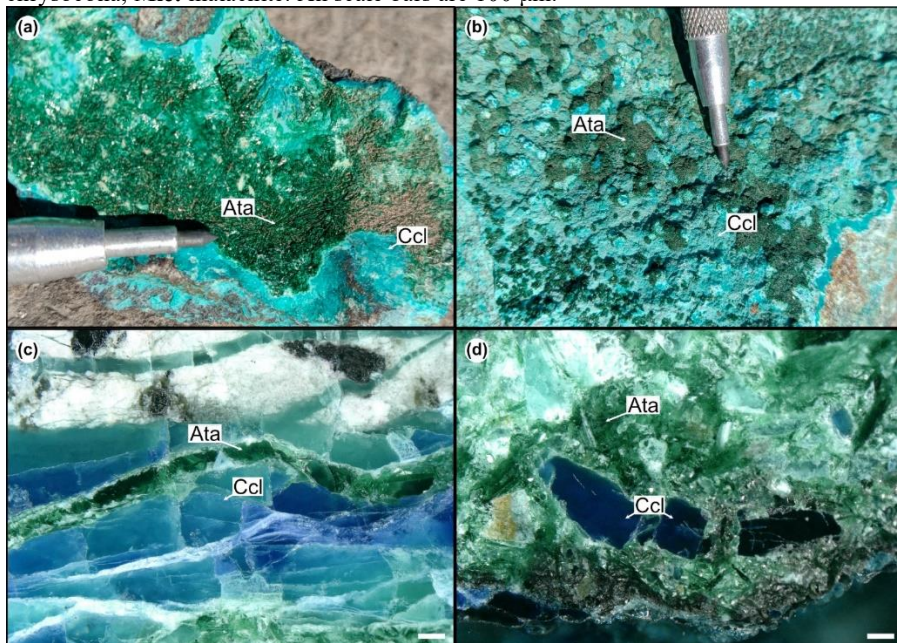
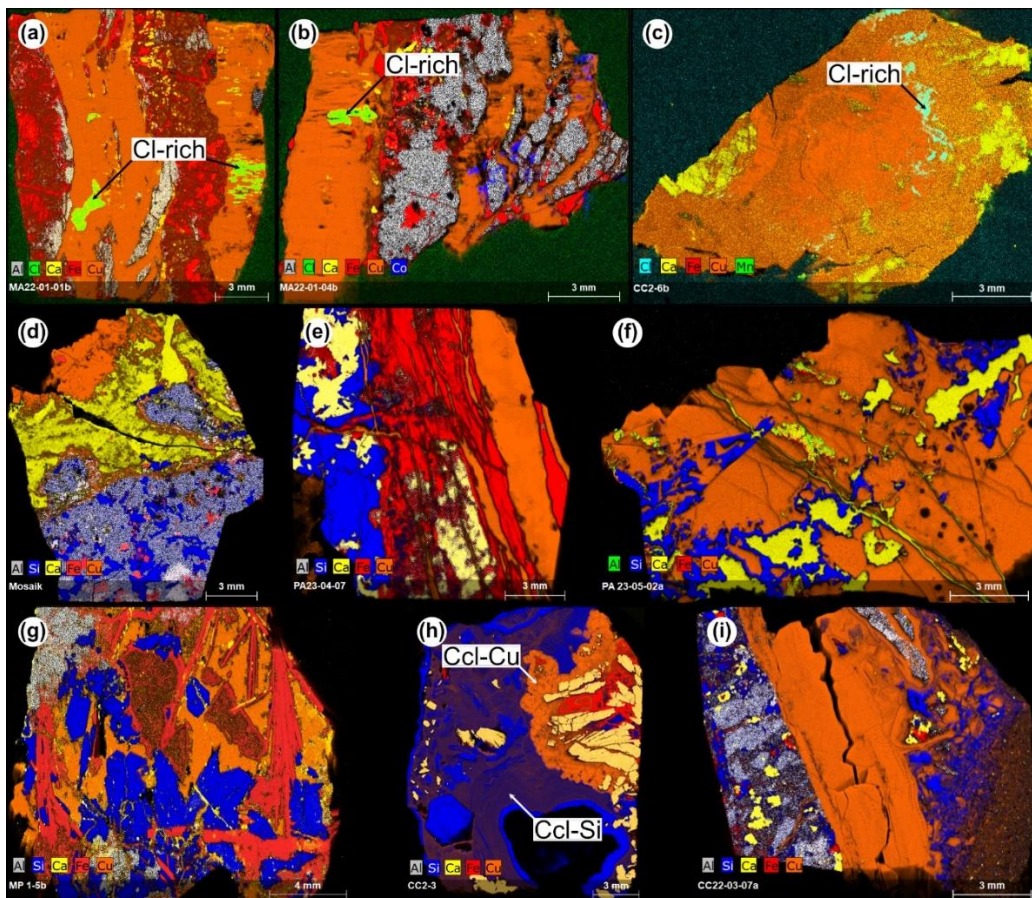


Figure 5. Atacamite textures. **(a-b)** Photographs of thin crust of atacamite over chrysocolla. **(a)** Sample MI23-04-17. **(b)** Sample CC22-08-06. **(c-d)** Photomicrograph of sample MI23-07-07. **(e)** Vein of atacamite cutting a vein of chrysocolla. **(d)** A chrysocolla clast fragmented by atacamite. **Ata:** atacamite, **Ccl:** chrysocolla. All scale bars are 100 µm.



200 4.2 μ XRF geochemical maps

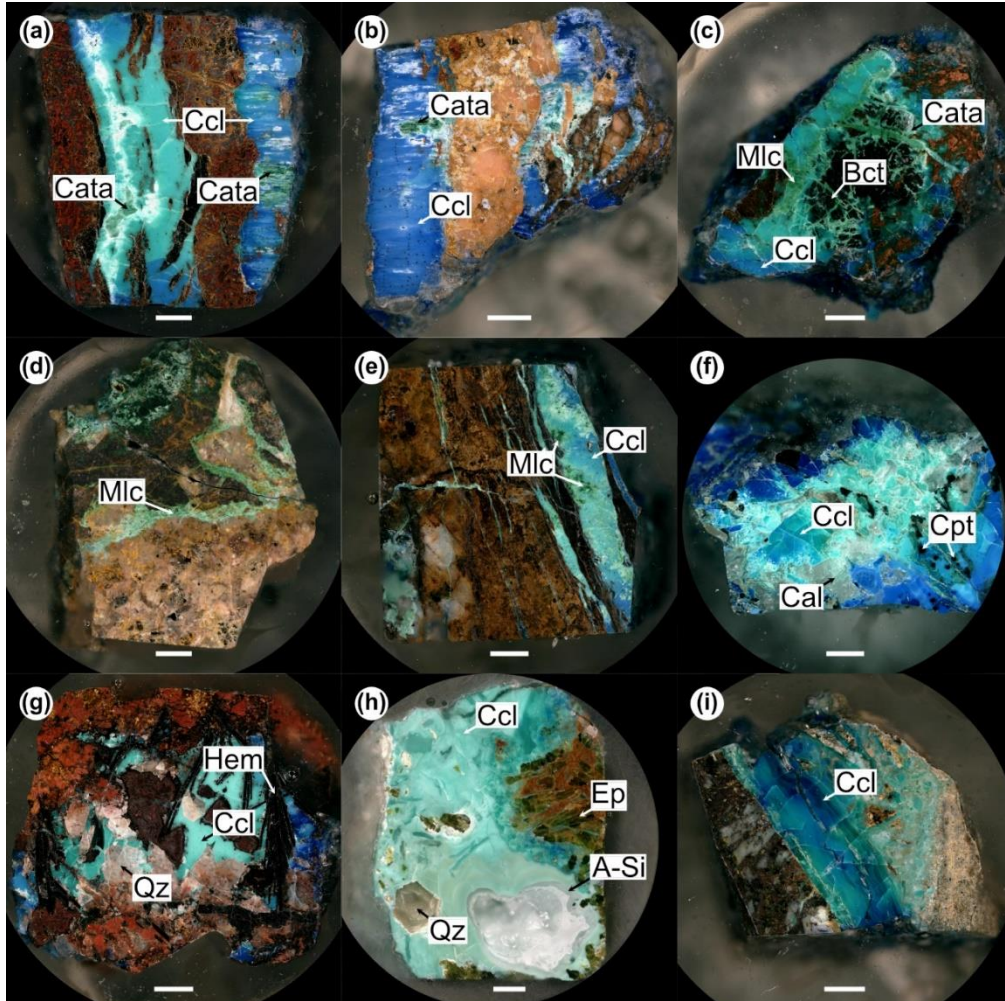
Nine samples were mapped using μ XRF. In three samples we identified a chlorine-rich mineral surrounded by chrysocolla (Fig. 6a-c). The samples have variable silica, aluminium, calcium, iron, manganese and cobalt content (Fig. 6a-i). The μ XRF analysis also shows that the sample CC2-3 has two kinds of chrysocolla that differ in the silica and copper content (Fig. 6h).



205 **Figure 6.** Results of μ XRF analyses of the samples: (a) MA22-01-01b; (b) MA22-01-01b; (c) CC2-6b; (d) PA23-01-11; (e) PA23-04-07; (f) PA23-05-02a; (g) MP1-5b; (h) CC2-3; (i) CC22-03-07a. **Cl-rich:** chlorine-rich mineral, **Ccl-Cu:** Cu-rich chrysocolla, **Ccl-Si:** Si-rich chrysocolla. The legend of colours is defined for each sample.

4.3 Raman spectroscopy

The mineral that is characterised by its striking chlorine content is clinoatacamite (Fig. 7a-c). Besides chrysocolla, atacamite and clinoatacamite, the copper supergene mineralisation is composed by brochantite, malachite and copper pitch (Fig. 7c-f). The silica, aluminium, calcium and iron content measured with μ XRF is related to the host rock and some specific minerals (Fig. 7a-i). Silica is associated with quartz and amorphous silica (Fig. 7g-h). The calcium is related to calcite (Fig. 7f) and epidote (Fig. 7h). The iron content is associated with iron oxide such as hematite (Fig. 7g). All LA-ICP-MS analysis were targeted on chrysocolla and malachite.



215

Figure 7. (a-i) Reflected light photographs of samples of figure 6. **Ccl:** chrysocolla, **Cata:** clinoatacamite, **Mic:** malachite, **Bct:** brochantite, **Cal:** calcite, **Cpt:** copper pitch, **Qz:** quartz, **Hem:** hematite, **Ep:** epidote, **A-Si:** amorphous silica, **Qz:** quartz. All scale bars are 2 mm.

4.4 LA-ICP-MS U-Pb dating

220 A total of 66 samples were measured in five sequences to define the U-Pb ratios and the viability of U-Pb dating in chrysocolla. After these measurements, 26 samples were re-analysed, considering the texture and setting more laser spots per sample. Many samples reveal extremely young, inferred ages or present uncertainties larger than the apparent age. From these 26 samples, we obtained seven samples with reliable ages (Table 1) (Figs. 8 and 9). All dates are calculated from multiple spot analyses, ranging from 34 to 81 spots per date. The majority of the analyses have U concentrations between \sim 1 and 355 $\mu\text{g g}^{-1}$, with an average of 60 $\mu\text{g g}^{-1}$. Following these results, we re-analysed the seven samples by targeting other spots, to find out whether other ages are obtained in different parts of the sample. From the seven samples, in only three samples we got new reliable results (Table 1) (Fig. 9). In the other four samples we got extremely young, inferred ages or

225



uncertainties larger than the apparent age. Moreover, we prepared duplicate mounts (a second resin block from the same rock) for three out of the seven previous samples to validate reproducibility of the obtained ages. However, none of the 230 duplicates give a reliable age.

Table 1: U-Pb ages of samples from the Coastal Cordillera.

Sample	Site	UTM Coordinates		Elevation (m a.s.l.)	Mineral	Age (Ma)	Age uncertainty (Ma)	Y- intercept (Ma)	Y-intercept uncertainty (Ma)	MSWD	n
		Latitude	Longitude								
Marimaca											
MA22-01-01b	MA22-01	375454	7435361	1101	Chrysocolla	0.32	0.11	0.704	0.004	1.18	81/81
MA22-01-04b	MA22-01	375454	7435361	1101	Chrysocolla	1.1	0.2	0.814	0.023	2.52	54/54
					Chrysocolla	0.39	0.30	0.748	0.031	1.34	30/30
					Chrysocolla	0.58	0.20	0.807	0.037	1.67	21/21
Caleta El Cobre											
CC22-03-07a	CC22-03b	352945	7316163	1565	Chrysocolla	0.046	0.027	0.801	0.004	1.4	69/69
CC2-3	CC22-03c	352343	7317058	1465	Chrysocolla	8.4	1.2	0.939	0.076	0.83	21/21
					Chrysocolla	0.50	0.37	0.842	0.014	0.54	14/17
					Chrysocolla	5.5	1.3	0.816	0.032	1.43	44/47
CC22-06-01	CC22-06	350683	7322721	821	Chrysocolla	0.64	0.40	0.806	0.027	1.27	65/65
Paposo											
PA23-01-11	PA23-01c	371128	7245818	2084	Malachite	7.7	0.7	0.739	0.006	1.73	13/13
PA23-04-07	PA23-04c	358909	7233519	1040	Chrysocolla	0.15	0.04	0.841	0.003	1.30	53/58
					Chrysocolla	0.12	0.11	0.838	0.010	1.31	36/36

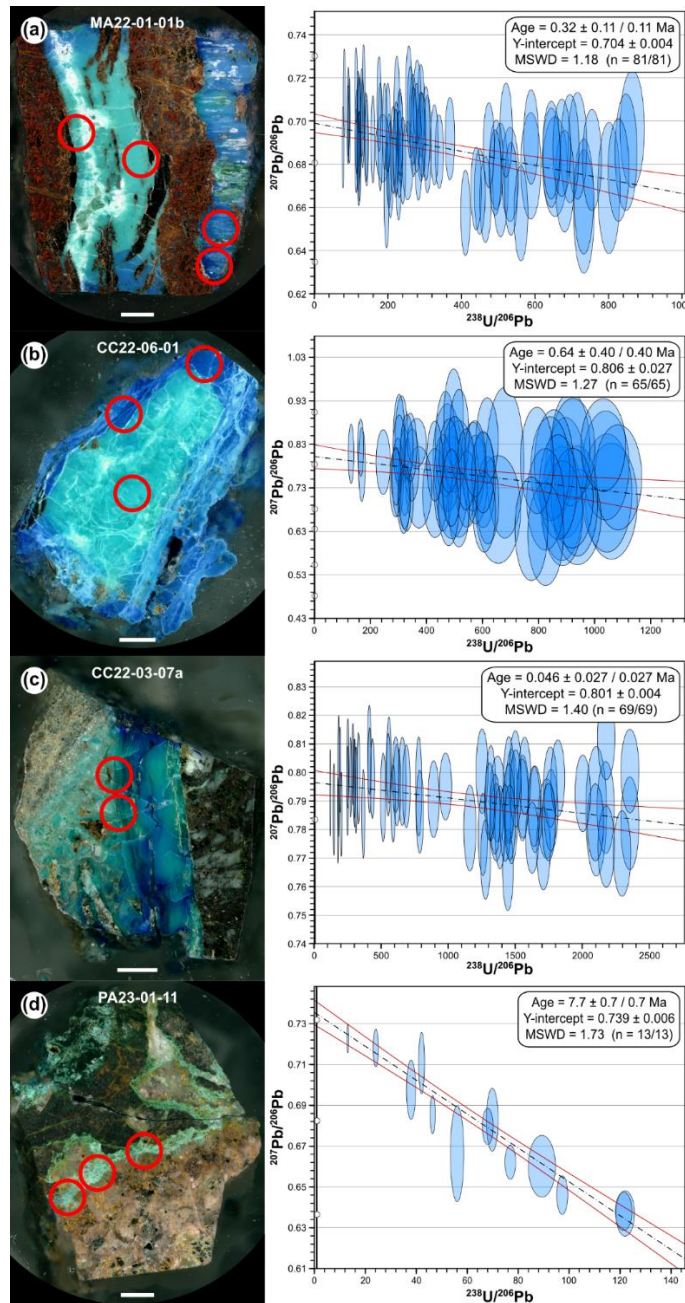


Figure 8. LA-ICP-MS U-Pb results. The red circles show the sites of the analyses. The white bars are 2mm. Uncertainty ellipses are 2s. Y intercept and mean square weighted deviation are shown. **(a)** sample MA22-01-01b; **(b)** sample CC22-06-01; **(c)** sample CC22-03-07a; **(d)** sample PA23-01-11.

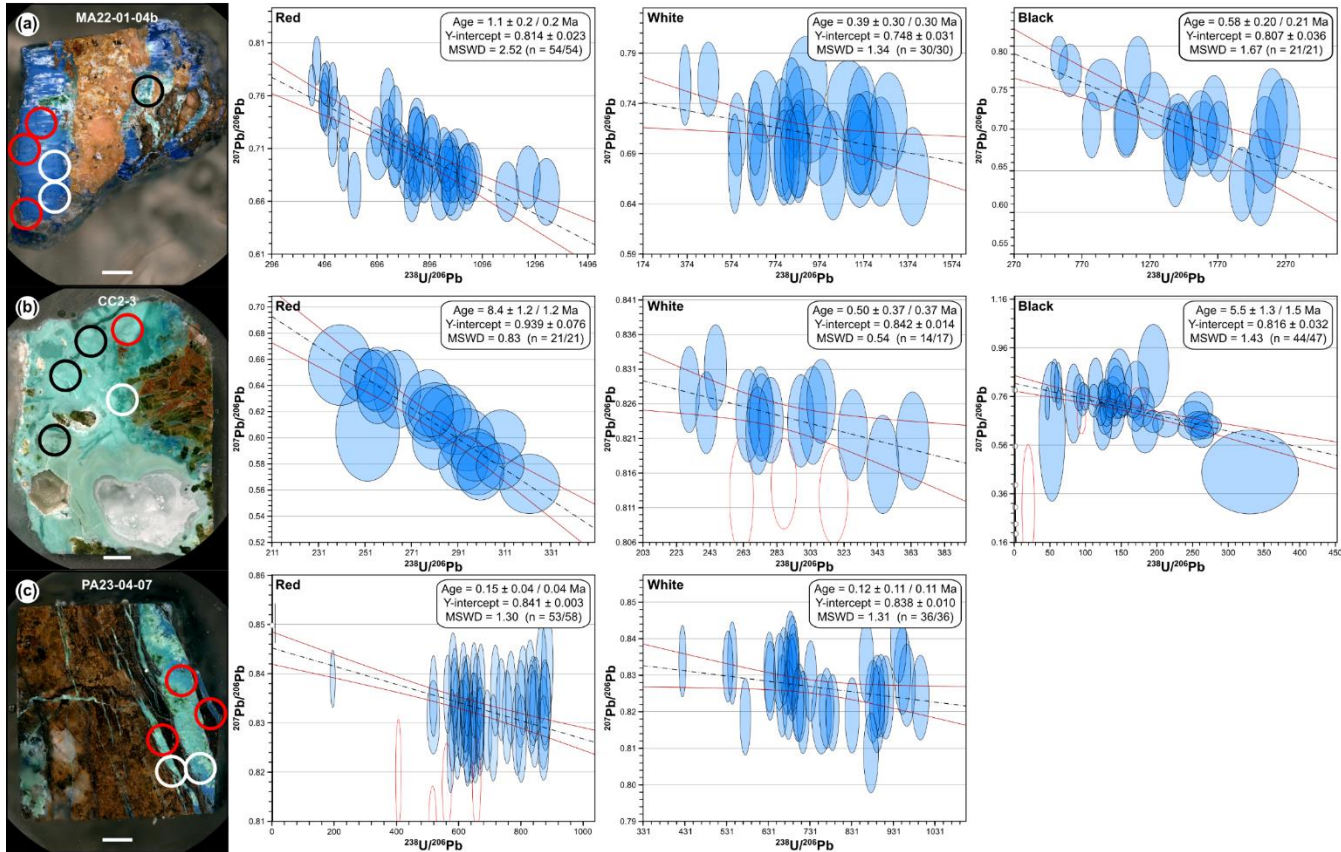


Figure 9. LA-ICP-MS U-Pb results. In each sample, the circles show the sites of the analyses. The red and white circles show the sites of the first analyses, while the black circles show the second analyses. The white bars are 2mm. Uncertainty ellipses are 2s. Y intercept and mean square weighted deviation are shown. **(a)** sample MA22-01-04b; **(b)** sample CC2-3; **(c)** sample PA23-04-07.

240

The obtained U-Pb ages in chrysocolla and malachite range from 0.046 ± 0.027 to 8.4 ± 1.2 Ma. Only for the Michilla area (Fig. 2b) we did not get any reliable U-Pb age (Table 1). In the Marimaca area, sample MA22-01-01b yielded an age of 0.32 ± 0.11 Ma (Fig. 8a), whereas sample MA22-01-04b yielded three ages ranging from 0.39 ± 0.30 to 1.1 ± 0.2 Ma (Fig. 9a). In the Caleta El Cobre, sample CC22-06-01 yielded an age of 0.64 ± 0.40 Ma (Fig. 8b), sample CC22-03-07a yielded an age of 0.046 ± 0.027 Ma (Fig. 8c), and sample CC2-3 yielded three ages ranging from 0.50 ± 0.37 to 8.4 ± 1.2 Ma (Fig. 9b). In the Paposo area, sample PA23-01-11 yielded an age of 7.7 ± 0.7 Ma (Fig. 8d), whereas sample PA23-04-07 yielded two ages: 0.12 ± 0.11 Ma and 0.15 ± 0.04 Ma (Fig. 9c). The sample CC2-3 presents two types of chrysocolla with different textures and different ages (Fig. 10). The massive chrysocolla has an age of 8.4 ± 1.2 Ma (MSWD = 0.83; n = 21; Fig. 10d) and the botryoidal chrysocolla an age of 0.50 ± 0.37 Ma (MSWD = 0.54; n = 14; Fig. 10f).

245

250

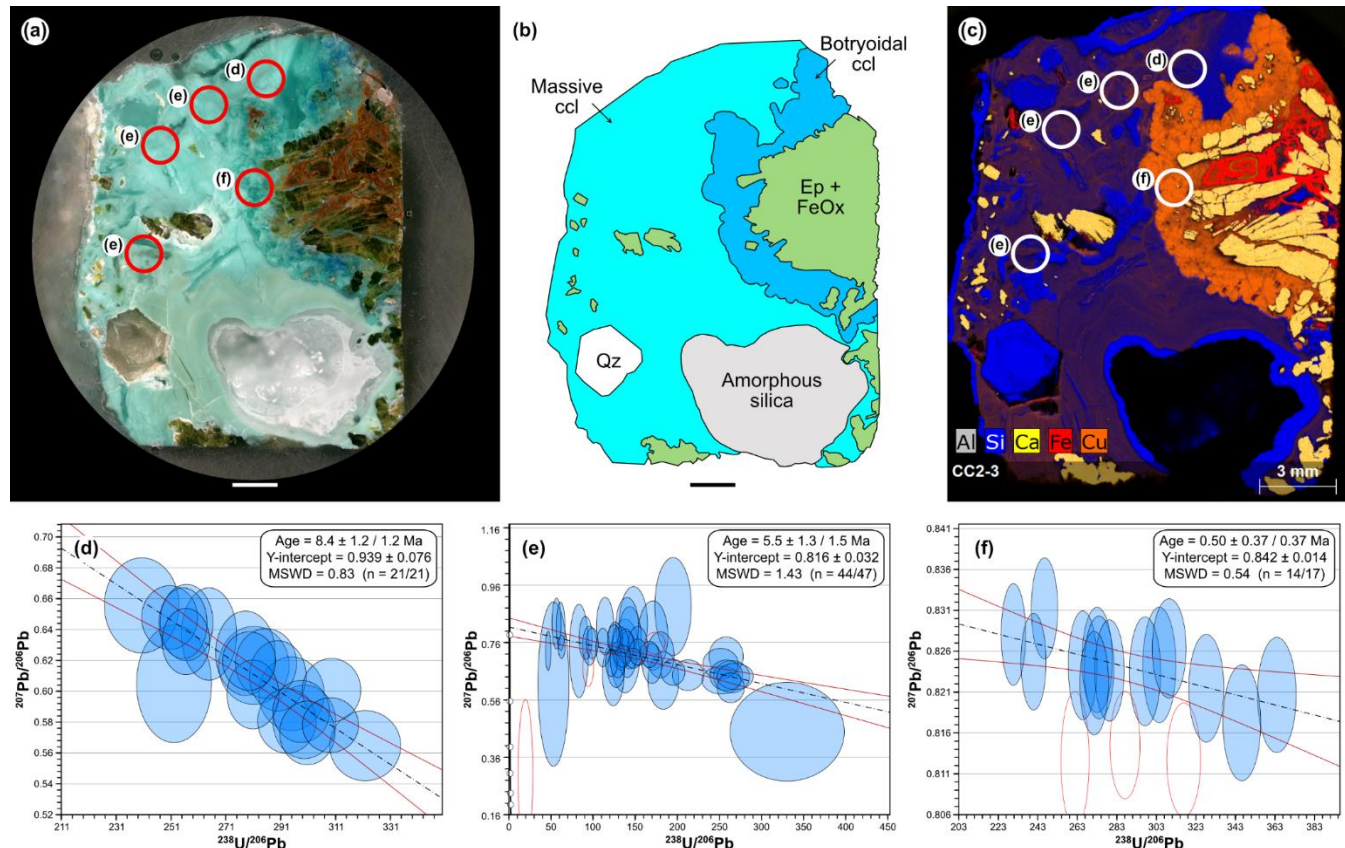


Figure 10. Sample CC2-3. (a) Reflected light image. It is possible to identify two chrysocolla: one massive and the other botryoidal. Scale bar is 2mm. (b) Schematic model showing the mineralogy of the sample. **Light blue:** massive chrysocolla; **blue:** botryoidal chrysocolla; **green:** epidote and iron oxide; **white:** quartz; **grey:** amorphous silica. Scale bar is 2mm. (c) μ XRF showing the distribution of specific chemical elements. Note that the massive chrysocolla had more silicon and less copper content than the botryoidal chrysocolla. (d–e) Results of LA-ICP-MS U–Pb dating of massive chrysocolla. (f) Results of LA-ICP-MS U–Pb dating of botryoidal chrysocolla. Uncertainty ellipses are 2s

5 Discussion

5.1 Mineral paragenesis

The Pourbaix diagram for copper minerals shows that chrysocolla and atacamite precipitate in the same thermodynamic conditions of other copper minerals and its precipitation is controlled by the concentration of Si and Cl in the system (Dold, 2006) (Fig. 11). The chemical composition of the mineralising fluid can explain why other copper supergene minerals such as brochantite and malachite, are scarce in the studied samples (Fig. 7). This is because the precipitation of brochantite and malachite are controlled by the concentration of sulphur and carbonate in the fluid. Besides, chrysocolla and atacamite are the final minerals to precipitate in supergene copper profiles (Dold et al., 2023). In the Paposo area, we obtain an age of 7.7 ± 0.7 Ma in malachite (PA23-01-11) and an age of 0.14 ± 0.04 Ma in chrysocolla (PA23-04-07) (Fig. 12), indicating that chrysocolla precipitated after malachite. Textural relationship shows that chrysocolla in the studied areas replace malachite



(Fig. 4c-d). In manto- and vein-type deposits in the Coastal Cordillera, it has been described that chrysocolla precipitate later than atacamite (Kojima et al., 2003; Tristá and Kojima, 2003). Nevertheless, the textural relationship between chrysocolla and atacamite found in our samples indicates that the atacamite is formed later than the chrysocolla (Fig. 5). Besides, the ages obtained on chrysocolla are older than those yielded in atacamite by Reich et al. (2009) in deposits from the Coastal Cordillera (Fig. 13). The presence of atacamite in the samples is interpreted as the final stage for copper mineralisation in the Coastal Cordillera triggered by the reaction between Cl-rich fluid and chrysocolla described in Eq. (1). The origins of these fluid are two: (1) fluid enriched with chloride as result of evaporation under hyperarid climate (Reich et al., 2008; Lambiel et al., 2023); or (2) saline groundwater that flow through faults (Cameron et al., 2010; Dold et al., 2023).

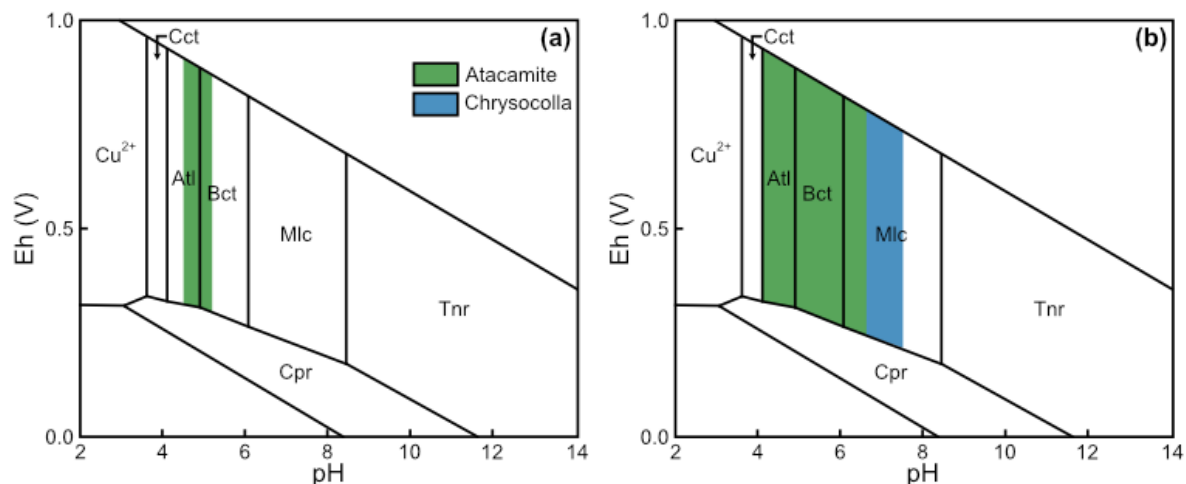
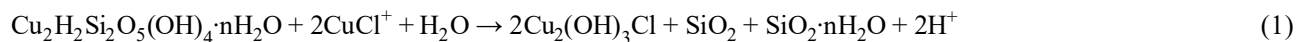


Figure 11. Pourbaix diagram of copper minerals to explain the mineralogy in the study areas. Pourbaix diagram of the system Cu-C-S-Si-O-OH showing stability fields of Cu-minerals at 25 °C and 1 atm. **Cct:** chalcantite; **Atl:** antlerite; **Bct:** brochantite; **Mlc:** malachite; **Tnr:** tenorite; **Cpr:** cuprite (modified from Guilbert and Park, 1986). **(a)** Stability field of atacamite (in green) with 14.3 mM Cu, 1.99 mM Cl and 1.81 mM Si at 25 °C and 1 bar. **(b)** Stability fields of atacamite (in green) and chrysocolla (in blue) with 14.3 mM Cu, 56.35 mM Cl and 70 mM Si at 25 °C and 1 bar.

5.2 U-Pb ages

Some of the obtained apparent U-Pb ages are extremely young (less than 1 Ma). A previous work conducting LA-ICP-MS U-Pb dating in Mn-rich chrysocolla, also known as copper pitch, suggests that the Pb-loss in the copper pitch occurs because the mineral structure is unable to keep the Pb after mineral precipitation (Kahou et al., 2021). Copper pitch is a mineraloid consisting of chrysocolla with co-precipitated birnessite ($(\text{Na},\text{Ca})_{0.5}(\text{Mn}^{4+},\text{Mn}^{3+})_2\text{O}_4 \cdot 1.5\text{H}_2\text{O}$) (Schwartz, 1934; Throop and Buseck, 1971; Dold et al., 2023). The age spread observed in Mn-rich chrysocolla can be explained by a complex behaviour of Pb in this mineraloid during the interaction of post-crystallisation fluid events (Kahou et al., 2021). Nevertheless, in the studied samples there is no evidence of Pb-loss in chrysocolla and malachite, so the Pb-loss is discarded as an explanation for the obtained ages.



The sample CC2-3 shows the most complex result with three different ages (8.4 ± 1.2 Ma; 5.5 ± 1.3 Ma; 0.50 ± 0.37 Ma) (Fig. 10) and two types of chrysocolla: one with a massive texture, a higher silica content (Fig. 10c) and the oldest ages (8.4 ± 1.2 Ma; 5.5 ± 1.3 Ma), and other with a botryoidal texture, a lower silica content (Fig. 10c) and the youngest age (0.50 ± 0.37 Ma) (Fig. 10a-b). The age dispersion measured within the massive chrysocolla (8.4 ± 1.2 Ma and 5.5 ± 1.3 Ma) might be explained by different precipitation process (Fig. 10d-e). According to the textural relationship, the botryoidal chrysocolla is the first to precipitate, because zoned monomineralic bands such as the observed on this chrysocolla are evidence of mineral growth in open spaces into fluid-filled voids (Craig and Vaughan, 1981). Nevertheless, according to the obtained U-Pb age, this botryoidal chrysocolla seems to be younger than the surrounding chrysocolla (Fig. 10f). In consequence, the ages younger than 1 Ma, obtained in this work and the age dispersion found in samples MA22-01-04b and CC2-3 (Fig. 9a-b) are consequence of recent supergene process in the Coastal Cordillera.

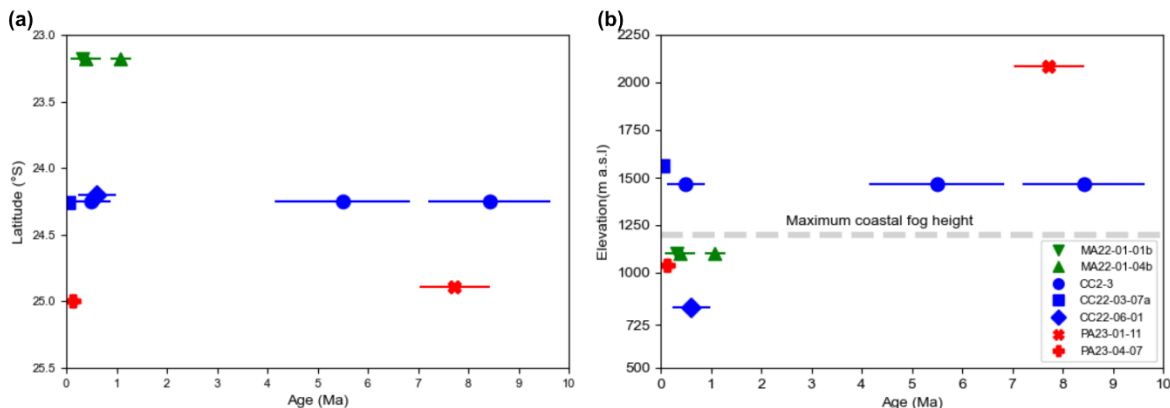


Figure 12. (a) The obtained U-Pb ages are plotted against the latitude of sampling points. (b) The obtained U-Pb ages are plotted against the elevation of sampling points. The grey dashed line shows the maximum height that can reach the coastal fog according by Schween et al. (2022). The symbols of samples for both graphs are showing in graph (b). Uncertainty of samples is 2σ .

5.3 Sample location and coastal fog influence

The study sites are located on the western side of the Coastal Cordillera (Figs. 1 and 2). The dated samples were taken from abandoned mine sites with an altitude that range from 821 to 2084 m a.s.l. (Table 1). Comparing the obtained ages vs latitude, it is possible to observe that young ages are present at all sampling sites where reliable U-Pb age were obtained, and the old ages are only in the southern sampling sites (Fig. 12a). The age vs elevation graph shows that in Caleta El Cobre and Paposo, where two samples were dated at different elevations, the older age corresponds to the higher altitude and the younger age to the lower one (Fig. 12b). In Marimaca, we did not obtain samples at different altitude, and both samples are below the coastal fog influence (Fig. 12b). In Caleta El Cobre area, the sample CC2-3 was taken at 1465 m a.s.l. and have an age of 8.4 ± 1.2 Ma while the sample CC22-06-01 were taken at 821 m a.s.l. and have an age of 0.61 ± 0.38 Ma (Fig. 12b). In Paranal area the sample PA23-01-11 were taken at 2084 m a.s.l. and have an age of 7.7 ± 0.7 Ma while the sample PA23-04-07 were taken at 1024 m a.s.l. and range from 0.12 ± 0.11 to 0.14 ± 0.04 Ma (Fig. 12b). In consequence, we suggest,



based on our limited number of samples from the Coastal Cordillera, that the elevation of the samples have more influence on the mineralisation ages than the latitude (Fig. 12). This relation between elevation and age could be related to the persistent presence of coastal fog, locally named *camanchaca*, that is a characteristic of the Coastal Cordillera in northern Chile (Cereceda et al., 2002; Rech et al., 2003; Schween et al., 2022). The coastal fog provides fresh water that help to develop ecosystems and drive surface processes (Cereceda et al., 2002; Dunai et al., 2020; Schween et al., 2022). The coastal fog is restricted to a height range from 300 to 1100 m a.s.l. in winter and from 600 to 1200 m a.s.l. in spring, and can reach 50 km inland through corridors formed within the Coastal Cordillera (Cereceda et al., 2002; Rech et al., 2003; Schween et al., 2022; Lobos-Roco et al., 2024). The majority of young ages are within these height ranges (Fig. 12b), and all dated samples are within the inland extent of coastal fog influence (Fig. 2). The fog occurrence and fog water availability along the Coastal Cordillera varies in time scales from diurnal to interannual (Larrain et al., 2002; Cereceda et al., 2008; Garreaud et al., 2008). Several studies along the coast of northern Chile have reported average annual fog water fluxes that range from 7 mm per day to 0.16 mm per day (Larrain et al., 2002; Cereceda et al., 2008; Carvajal et al., 2022). The measurements varies within the year reaching the maximum fog water fluxes during winter and the minimum during summer (Cereceda et al., 2008; del Río et al., 2018; Carvajal et al., 2022; Schween et al., 2022). The fog cloud cover and fog water fluxes are controlled by the El Niño Southern Oscillation (ENSO) (Garreaud et al., 2008; del Río et al., 2018). To the north of ~25°S during ENSO (+) (El Niño) there is a significantly higher fog cloud cover and fog water fluxes during both summer and winter when compared to ENSO (-) (La Niña) years (Garreaud et al., 2008; del Río et al., 2018). In Alto Patache (20°49'S, 70°09'W; 850 m a.s.l.), during September of 1997 (very strong El Niño) amount of fog-precipitation was collected of up to 28.4 mm per day (~852 mm per month), that is the highest month fog water collection registered in the area (Muñoz-Schick et al., 2001). Evenstar et al., 2024 propose that to develop supergene mineralisation, is required a precipitation rate above 120 mm per year. Nevertheless, this value is an average over a long-time scale, estimated on base of groundwater recharge; therefore, it is not necessary a minimum value to trigger supergene mineralisation. It is possible, that under the right conditions, the MAR is much lower to develop supergene mineralisation in the Coastal Cordillera. Besides, has been proposed that the supergene mineralisation in the Atacama Desert could be formed in arid conditions (Clarke, 2006), and that the supergene mineralisation is an ongoing process after the onset of hyperaridity (Reich et al., 2009; Bissig and Riquelme, 2010; Morales-Leal et al., 2023). Considering the amount of fog water collected in Alto Patache it is possible to propose that during very strong El Niño periods there might be enough water to trigger supergene mineralisation in the Coastal Cordillera.

Calculated uplift rates of the Coastal Cordillera range from 45 m Myr⁻¹ during the upper Cretaceous to Paleocene (Juez-Larré et al., 2010) to 600 m My⁻¹ during the Pleistocene (Martinod et al., 2016). With these uplift rates, it is possible that the highest samples (CC2-3 and PA23-01-11; Fig.12b) could had been uplifted above the fog zone influence after the supergene mineralisation process, and in consequence, get disconnected to any moisture supply causing supergene activity.



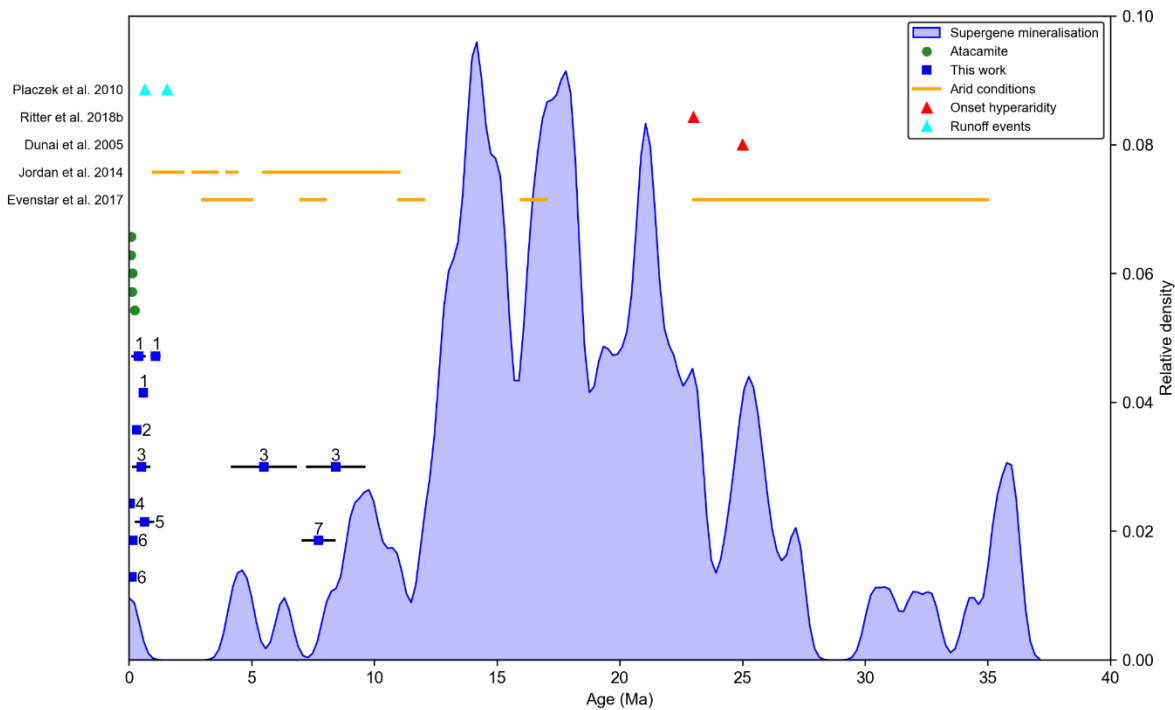
5.4 Palaeoclimate significance

350 Supergene mineralisation studies, mainly from the Central Depression and Precordillera propose that the supergene mineralisation in the Atacama Desert was active from Eocene to Late Pleistocene and occurred in two stages (Hartley and Rice, 2005; Arancibia et al., 2006; Reich et al., 2009; Evenstar et al., 2024) (Fig. 13). The first stage started 45 Ma and lasted until 5 Ma, with a scarce record of supergene minerals between 9 and 5 Ma (Arancibia et al., 2006; Reich et al., 2009). This scarce record between 9 and 5 Ma has been used to propose a Miocene onset of the hyperaridity in the Atacama Desert
355 (Sillitoe and McKee, 1996). The second stage started at 2 Ma and lasted until the Late Pleistocene, and it is restricted to the atacamite precipitation (Reich et al., 2009). From both stages there are only four ages from the Coastal Cordillera: 21.1 ± 0.6 Ma using K-Ar in supergene alunite (Sillitoe and McKee, 1996); 75.3 ± 0.4 , 84 ± 11 and 143 ± 29 ka using Th-U in gypsum intergrowth with atacamite (Reich et al., 2009) (Fig. 1). The Th-U ages has been described as the youngest age recorded in a supergene profile in the Atacama Desert (Reich et al., 2009). Nevertheless, gypsum is formed under arid conditions (Murray,
360 1964; Sofer, 1978) and is not directly related to the supergene copper mineralisation process. Furthermore, atacamite is the final part of the mineralisation in the Coastal Cordillera, and to precipitate it require Cl-rich fluid as result of evaporation under hyperarid climate (Reich et al., 2008; Lambiel et al., 2023). If we only consider the ages obtained in copper supergene minerals, the obtained U-Pb chrysocolla ages in this work are the youngest ages recorded in supergene deposits from the Atacama Desert. The oldest ages obtained in this work (Sample CC2-3: 8.4 ± 1.2 Ma, 5.5 ± 1.3 Ma; PA23-01-11: 7.7 ± 0.7
365 Ma; Fig. 13a) are in the time gap between 9-5 Ma, where the record of supergene minerals is scarce. The rest of the samples are in the second stage of mineralisation with exception of the sample MA22-01-04b (Fig. 13). The youngest age of supergene mineralisation in a deposit is interpreted as the last time with sufficient moisture (above 120 mm per year; Evenstar et al., 2024), so it will reflect the transition from arid towards hyperarid conditions (Alpers and Brimhall, 1988; Sillitoe and McKee, 1996; Hartley and Rice, 2005). However, even short-lived intervals with sufficient precipitation could
370 have triggered supergene activity and the associated chrysocolla precipitation in the Coastal Cordillera within a predominantly hyperarid climate that has persisted for millions of years. The obtained ages on copper supergene minerals are young (from 8.4 ± 1.2 Ma to 0.046 ± 0.027 Ma) and are consistent with the model that proposes that the supergene mineralisation is an ongoing process after the onset of hyperaridity in the Coastal Cordillera (Reich et al., 2009; Bissig and Riquelme, 2010; Morales-Leal et al., 2023). Furthermore, the results suggest that wetter period occurred in the Coastal
375 Cordillera but did not reactivate supergene activity in the Precordillera. This implies that the supergene mineralisation processes in the Coastal Cordillera and those in the Precordillera and Central Depression were triggered by different water sources.

Other proxies have been used to point the onset of hyperaridity in the Coastal Cordillera. Cosmogenic nuclides ages from the
380 Coastal Cordillera at $\sim 19^{\circ}34'S$ (Dunai et al., 2005) and at $21^{\circ}30'$ (Ritter et al., 2018a) indicate the onset of hyperaridity at 25 Ma and at 23 Ma respectively (Figs. 1 and 13). Also, in the Coastal Cordillera at $\sim 19^{\circ}34'S$, were registered pluvial episodes prior to 20 Ma, 14 Ma and 9 Ma using cosmogenic nuclides ages (Dunai et al., 2005). Erosion rate data at $\sim 24^{\circ}S$ support a

Miocene onset of hyperaridity in the Coastal Cordillera (Placzek et al., 2014) (Fig. 1). Sedimentological studies in the Coastal Cordillera at $\sim 26^{\circ}\text{S}$ propose that pluvial activity capable to trigger stream incisions were reduced to insignificant levels in the late Pliocene to early Pleistocene as consequence of the onset of hyperaridity (Amundson et al., 2012) (Fig. 1).

385 Nevertheless, cosmogenic nuclides data support that the Coastal Cordillera near the $\sim 24^{\circ}\text{S}$ (Fig. 1) has remained
 geomorphologically active during the Pleistocene triggered by rainfalls that come from the south (Placzek et al., 2010) (Fig.
 13). The differences in the ages proposed for the onset of hyperaridity in the Atacama Desert can be explained by the
 regional distribution of studies and the sensitivity of the proxies used (Ritter et al., 2018a).



390 **Figure 13.** Comparison of palaeoclimatic record with the obtained U-Pb ages. Numbers indicate identical sample: (1) MA22-01-04b, (2) MA22-01-01b, (3) CC2-3, (4) CC22-03-07a, (5) CC22-06-01, (6) PA23-04-07, (7) PA23-01-11. The data to create the probability curve of
 395 supergene mineralisation was taken from: Gustafson and Hunt (1975), Alpers and Brimhall (1988), Sillitoe and McKee (1996), Marsh et al. (1997), Mote et al. (2001), Bouzari and Clark (2002), Arancibia et al. (2006) Warren et al. (2008), Reich et al. (2009), Bissig and Riquelme (2010), Perelló et al. (2010), Hervé et al. (2012), Riquelme et al. (2018) and Kahou et al. (2021). The onset hyperaridity from Dunai et al. (2005) was registered at 19°35'S in the Coastal Cordillera (Fig. 1). The onset hyperaridity from Ritter et al. (2018b) was registered at 21°30'S in the Coastal Cordillera (Fig. 1). and Evenstar et al. (2017) were registered in the Central Depression (Fig. 1). The atacamite ages are the Th-U in gypsum intergrowth with atacamite obtained by Reich et al. (2009). The obtained ages of this work include the uncertainty (2s).

400 Cosmogenic nuclides ages from the Central Depression support that, despite a predominantly hyperarid climate in the Atacama Desert, punctual and episodic wetter episodes occurred (Jordan et al., 2014; Evenstar et al., 2017; Ritter et al., 2018b). Proposed pluvial events in the Central Depression have been dated prior to 35-23 Ma, 17-16 Ma, 12-11 Ma, 8-7 Ma, 5.5-4.5 Ma, 4-3.6 Ma, 2.6-2.2 Ma, 2.92 ± 0.24 Ma, 1.27 ± 0.47 Ma, 540 ± 160 ka, 392 ± 37 ka and 274 ± 74 ka. (Jordan et al., 2014; Evenstar et al., 2017; Ritter et al., 2018b). Although some of these ages overlap with those obtained for



405 chrysocolla and malachite in this study, the pluvial events are associated with Andean-derived precipitation, whereas the copper supergene mineralisation analysed here more likely reflects episodes of pluvial and/or intense fog activity in the Coastal Cordillera.

6 Conclusions

Some of the obtained ages in this study are extremely young (less than 1 Ma); nevertheless, these results are interpreted as 410 precipitation ages of chrysocolla and are evidence of recent supergene processes episodes in the Coastal Cordillera.

Sporadic pluvial events and the coastal fog are proposed as the water sources to develop copper supergene mineralisation in the Coastal Cordillera. Fog water collection data in Alto Patache indicate that during very strong ENSO periods there is enough water to trigger the supergene mineralisation in the Coastal Cordillera. The ages of pluvial events recorded in Coastal Cordillera and Central Depression match with the obtained ages in this work. The majority of the young ages 415 correspond to samples collected within the elevation range and inland limit of the coastal fog penetration (Figs. 2 and 12). These pluvial events with intense fog activity could explain the obtained young ages (less than 1 Ma) in this work.

Although the pluvial events proposed for the Central Depression appear to coincide with the ages of chrysocolla and malachite obtained in this study, those events are linked to Andean-derived moisture and thus do not represent the water source of the supergene processes recorded in the Coastal Cordillera. The young precipitation ages of chrysocolla and 420 malachite in the Coastal Cordillera of Northern Chile are evidence that the supergene processes are more recent in the Coastal Cordillera than in the Precordillera, evidencing that the western parts along the Coastal Cordillera experience more precipitation and the influence of coastal fog to trigger the mineralisation processes.

The dating of chrysocolla using the U-Pb LA-ICP-MS method is feasible, but it is necessary to improve our understanding of Pb behaviour after chrysocolla precipitation.

425 Data availability

All data used in this work are provided in the Supplement.

Supplement

The supplement related to this article is available online at.



Author contributions

430 JRC: fieldwork, sample preparation, U-Pb analysis, data evaluation, manuscript writing. RA: fieldwork, U-Pb analysis, data evaluation, manuscript writing. BRP: data evaluation, manuscript writing. AG: U-Pb analysis, data evaluation. TD: fieldwork, data evaluation. EC: fieldwork, data evaluation. All authors reviewed the manuscript.

Competing interest

Co-author Tibor Dunai is an editor of Geochronology.

435 Acknowledgments

Stephan Opitz and Christoph Lenting for helping with the μ XRF and Raman, respectively, and Fernando Álvarez and Jorge García for helping with sample treatment, laboratory work, and XRD analyses are greatly acknowledged. Mario Tabilo for the assistance during the fieldworks in Michilla and Paposo. Beatriz Chacana for the help during the fieldwork in Caleta El Cobre. The authors acknowledge the help and assistance during the visit to the different mines: Sebastián Eade (Marimaca 440 Copper project), Yohani Araya (Cráter Mine in Paposo) and Yanira Muñoz (Chulin Mine in Caleta El Cobre).

Financial support

The project is funded by the Deutsche Forschungsgemeinschaft (DFG, German Research Foundation) Collaborative Research Centre 1211 Earth - Evolution at the Dry Limit (SFB 1211, Projektnummer 268236062), and the Chilean National Agency for Research and Development (ANID), via the scholarship program Doctorado Beca Nacional N°. 21242202 (J. 445 Ríos-Contesse).

References

Alpers, C. N. and Brimhall, G. H.: Middle Miocene climatic change in the Atacama Desert, northern Chile: Evidence from supergene mineralization at La Escondida, Geol. Soc. Am. Bull., 100, 1640–1656, [https://doi.org/10.1130/0016-7606\(1988\)100<1640:MMCCIT>2.3.CO;2](https://doi.org/10.1130/0016-7606(1988)100<1640:MMCCIT>2.3.CO;2), 1988.

450 Amundson, R., Dietrich, W., Bellugi, D., Ewing, S., Nishiizumi, K., Chong, G., Owen, J., Finkel, R., Heimsath, A., Stewart, B., and Caffee, M.: Geomorphologic evidence for the late Pliocene onset of hyperaridity in the Atacama Desert, Geol. Soc. Am. Bull., 124, 1048–1070, <https://doi.org/10.1130/B30445.1>, 2012.

Arancibia, G., Matthews, S. J., and Pérez de Arce, C.: K-Ar and $40\text{Ar}/39\text{Ar}$ geochronology of supergene processes in the Atacama Desert, Northern Chile: Tectonic and climatic relations, J. Geol. Soc. London., 163, 107–118,



455 <https://doi.org/10.1144/0016-764904-161>, 2006.
Barra, F., Reich, M., Selby, D., Rojas, P., Simon, A., Salazar, E., and Palma, G.: Unraveling the origin of the Andean IOCG clan: A Re-Os isotope approach, *Ore Geol. Rev.*, 81, 62–78, <https://doi.org/10.1016/j.oregeorev.2016.10.016>, 2017.

Bissig, T. and Riquelme, R.: Andean uplift and climate evolution in the southern Atacama Desert deduced from geomorphology and supergene alunite-group minerals, *Earth Planet. Sci. Lett.*, 299, 447–457,

460 <https://doi.org/10.1016/j.epsl.2010.09.028>, 2010.

Boric, R., Díaz, F., and Maksaev, V.: Geología y yacimientos metalíferos de la Región de Antofagasta, Servicio Nacional de Geología y Minería (SERNAGEOMIN), Santiago, Chile, 246 pp., 1990.

Bouzari, F. and Clark, A. H.: Anatomy, evolution, and metallogenic significance of the supergene orebody of the Cerro Colorado Porphyry Copper Deposit, I Región, Northern Chile, *Econ. Geol.*, 97, 1701–1740,

465 <https://doi.org/10.2113/gsecongeo.97.8.1701>, 2002.

Cameron, E. M., Leybourne, M. I., Reich, M., and Palacios, C.: Geochemical anomalies in northern Chile as a surface expression of the extended supergene metallogenesis of buried copper deposits, *Geochemistry Explor. Environ. Anal.*, 10, 157–169, <https://doi.org/10.1144/1467-7873/09-228>, 2010.

Carvajal, D., Mora-Carreño, M., Sandoval, C., and Espinoza, S.: Assessing fog water collection in the coastal mountain range of Antofagasta, Chile, *J. Arid Environ.*, 198, <https://doi.org/10.1016/j.jaridenv.2021.104679>, 2022.

Cereceda, P., Osses, P., Larrain, H., Farías, M., Lagos, M., Pinto, R., and Schemenauer, R. S.: Advective, orographic and radiation fog in the Tarapacá region, Chile, *Atmos. Res.*, 64, 261–271, [https://doi.org/10.1016/S0169-8095\(02\)00097-2](https://doi.org/10.1016/S0169-8095(02)00097-2), 2002.

Cereceda, P., Larrain, H., Osses, P., Farías, M., and Egaña, I.: The climate of the coast and fog zone in the Tarapacá Region, 475 Atacama Desert, Chile, *Atmos. Res.*, 87, 301–311, <https://doi.org/10.1016/j.atmosres.2007.11.011>, 2008a.

Cereceda, P., Larrain, H., Osses, P., Farías, M., and Egaña, I.: The spatial and temporal variability of fog and its relation to fog oases in the Atacama Desert, Chile, *Atmos. Res.*, 87, 312–323, <https://doi.org/10.1016/j.atmosres.2007.11.012>, 2008b.

Charrier, R., Pinto, L., and Rodríguez, M. P.: Tectonostratigraphic evolution of the Andean Orogen in Chile, *Geol. Soc. Spec. Publ.*, 21–114, <https://doi.org/10.1144/goch.3>, 2007.

480 Charrier, R., Farías, M., and Maksaev, V.: Evolución tectónica, paleogeográfica y metalogénica durante el cenozoico en los Andes de Chile Norte y Central e implicaciones para las regiones adyacentes de Bolivia y Argentina, *Rev. la Asoc. Geol. Argentina*, 65, 5–35, 2009.

Clark, A. H., Tosdal, R. M., Farrar, E., and Plazolles V., A.: Geomorphologic environment and age of supergene enrichment of the Cuajone, Quellaveco, and Toquepala porphyry copper deposits, southeastern Peru, *Econ. Geol.*, 85, 1604–1628,

485 <https://doi.org/10.2113/gsecongeo.85.7.1604>, 1990.

Clarke, J. D. A.: Antiquity of aridity in the Chilean Atacama Desert, *Geomorphology*, 73, 101–114, <https://doi.org/10.1016/j.geomorph.2005.06.008>, 2006.

Coira, B., Davidson, J., Mpodozis, C., and Ramos, V.: Tectonic and magmatic evolution of the Andes of northern Argentina



and Chile, *Earth Sci. Rev.*, 18, 303–332, [https://doi.org/10.1016/0012-8252\(82\)90042-3](https://doi.org/10.1016/0012-8252(82)90042-3), 1982.

490 Craig, J. R. and Vaughan, D. J.: *Ore microscopy and ore petrography.*, Wiley, New York, [https://doi.org/10.1016/s0892-6875\(96\)90069-2](https://doi.org/10.1016/s0892-6875(96)90069-2), 1981.

Crane, M. J., Sharpe, J. L., and Williams, P. A.: Formation of chrysocolla and secondary copper phosphates in the highly weathered supergene zones of some Australian deposits, *Rec. Aust. Museum*, 53, 49–56, <https://doi.org/10.3853/j.0067-1975.53.2001.1323>, 2001.

495 Dold, B.: Geochemical modeling of the exotic mineralization of the Exótica deposit at Chuquicamata, Chile, *Actas, XI Congr. Geológico Chil.*, 2, 247–250, 2006.

Dold, B., Caroline, M., and Lluís, P.: Genesis of the exotic chrysocolla — “copper pitch/wad” — atacamite/brochantite ore at the Exótica (Mina Sur) deposit, Chuquicamata, Chile, *Miner. Depos.*, 58, 569–591, 2023.

Dunai, T. J., González López, G. A., and Juez-Larré, J.: Oligocene-Miocene age of aridity in the Atacama Desert revealed by 500 exposure dating of erosion-sensitive landforms, *Geology*, 33, 321–324, <https://doi.org/10.1130/G21184.1>, 2005.

Dunai, T. J., Melles, M., Quandt, D., Knief, C., and Amelung, W.: Whitepaper: Earth – Evolution at the dry limit, *Glob. Planet. Change*, 193, <https://doi.org/10.1016/j.gloplacha.2020.103275>, 2020.

Evenstar, L., Dahlström, S., Hartley, A., McCuaig, T. C., Mather, A., and Shaw, J.: Global constraints on exhumation rates during porphyry copper formation and supergene enrichment: applications to exploration as illustrated from the Central 505 Andes, *Miner. Depos.*, 2024.

Evenstar, L. A., Mather, A. E., Hartley, A. J., Stuart, F. M., Sparks, R. S. J., and Cooper, F. J.: Geomorphology on geologic timescales: Evolution of the late Cenozoic Pacific paleosurface in Northern Chile and Southern Peru, *Earth-Science Rev.*, 171, 1–27, <https://doi.org/10.1016/j.earscirev.2017.04.004>, 2017.

FAO: Arid zone forestry: A guide for field technicians, FAO Forestry Paper 20, Food and Agriculture Organization of the 510 United Nations, Rome, 1989.

Frost, R. L. and Xi, Y.: Is chrysocolla $(\text{Cu},\text{Al})_2\text{H}_2\text{Si}_2\text{O}_5(\text{OH})_4 \cdot n\text{H}_2\text{O}$ related to spertiniite $\text{Cu}(\text{OH})_2?$ - A vibrational spectroscopic study, *Vib. Spectrosc.*, 64, 33–38, <https://doi.org/10.1016/j.vibspec.2012.10.001>, 2013.

García, F.: Geología del Norte Grande de Chile, in: *Symposium sobre Geosinclinal Andino*, 138, 1967.

Garreaud, R., Barichivich, J., Christie, D. A., and Maldonado, A.: Interannual variability of the coastal fog at Fray Jorge 515 relict forests in semiarid Chile, *J. Geophys. Res. Biogeosciences*, 113, 1–16, <https://doi.org/10.1029/2008JG000709>, 2008.

Gerdes, A. and Zeh, A.: Combined U-Pb and Hf isotope LA-(MC-)ICP-MS analyses of detrital zircons: Comparison with SHRIMP and new constraints for the provenance and age of an Armorican metasediment in Central Germany, *Earth Planet. Sci. Lett.*, 249, 47–61, <https://doi.org/10.1016/j.epsl.2006.06.039>, 2006.

Gerdes, A. and Zeh, A.: Zircon formation versus zircon alteration - New insights from combined U-Pb and Lu-Hf in-situ 520 LA-ICP-MS analyses, and consequences for the interpretation of Archean zircon from the Central Zone of the Limpopo Belt, *Chem. Geol.*, 261, 230–243, <https://doi.org/10.1016/j.chemgeo.2008.03.005>, 2009.

Gustafson, L. B. and Hunt, J. P.: The porphyry copper deposit at El Salvador, Chile, *Econ. Geol.*, 70, 857–912,



<https://doi.org/10.2113/gsecongeo.70.5.857>, 1975.

Hariu, T., Arima, H., and Sugiyama, K.: The structure of hydrated copper-silicate gels, an analogue compound for natural chrysocolla, *J. Mineral. Petrol. Sci.*, 108, 111–115, <https://doi.org/10.2465/jmps.121022c>, 2013.

525 Hartley, A. J. and Rice, C. M.: Controls on supergene enrichment of porphyry copper deposits in the Central Andes: A review and discussion, *Miner. Depos.*, 40, 515–525, <https://doi.org/10.1007/s00126-005-0017-7>, 2005.

Hartley, A. J., Mather, A. E., Jolley, E., and Turner, P.: Climatic controls on alluvial-fan activity, Coastal Cordillera, northern Chile, *Geol. Soc. Spec. Publ.*, 251, 95–116, <https://doi.org/10.1144/GSL.SP.2005.251.01.08>, 2005.

530 Hervé, M., Sillitoe, R. H., Wong, C., Fernández, P., Crignola, F., Ipinza, M., and Urzúa, F.: Geologic Overview of the Escondida Porphyry Copper District, Northern Chile, in: *Geology and Genesis of Major Copper Deposits and Districts of the World: A Tribute to Richard H. Sillitoe*, edited by: Hedenquist, J. W., Harris, M., and Camus, F., Society of Economic Geologists, Littleton, U. S. A., 55–78., <https://doi.org/10.5382/SP.16.03>, 2012.

Jordan, T. E., Kirk-Lawlor, N. E., Nicolás Blanco, P., Rech, J. A., and Cosentino, N. J.: Landscape modification in response 535 to repeated onset of hyperarid paleoclimate states since 14 Ma, Atacama Desert, Chile, *Geol. Soc. Am. Bull.*, 126, 1016–1046, <https://doi.org/10.1130/B30978.1>, 2014.

Juez-Larré, J., Kukowski, N., Dunai, T. J., Hartley, A. J., and Andriessen, P. A. M.: Thermal and exhumation history of the Coastal Cordillera arc of northern Chile revealed by thermochronological dating, *Tectonophysics*, 495, 48–66, <https://doi.org/10.1016/j.tecto.2010.06.018>, 2010.

540 Kahou, Z. S., Brichau, S., Poujol, M., Duchêne, S., Campos, E., Leisen, M., D'Abzac, F. X., Riquelme, R., and Carretier, S.: First U-Pb LA-ICP-MS in situ dating of supergene copper mineralization: case study in the Chuquicamata mining district, Atacama Desert, Chile, *Miner. Depos.*, 56, 239–252, <https://doi.org/10.1016/j.oregeorev.2021.104078>, 2021.

Kojima, S., Astudillo, J., Rojo, J., Tristá, D., and Hayashi, K. I.: Ore mineralogy, fluid inclusion, and stable isotopic characteristics of stratiform copper deposits in the coastal Cordillera of northern Chile, *Miner. Depos.*, 38, 208–216, 545 <https://doi.org/10.1007/s00126-002-0304-5>, 2003.

Kojima, S., Trista-Aguilera, D., and Hayashi, K. I.: Genetic aspects of the manto-type copper deposits based on geochemical studies of North Chilean deposits, *Resour. Geol.*, 59, 87–98, <https://doi.org/10.1111/j.1751-3928.2008.00081.x>, 2009.

Lafuente, B., Downs, R. T., Yang, H., and Stone, N.: The power of databases: The RRUFF project, *Highlights Mineral. Crystallogr.*, 1–29, <https://doi.org/10.1515/9783110417104-003>, 2016.

550 Larrain, H., Velásquez, F., Cereceda, P., Espejo, R., Pinto, R., Osses, P., and Schemenauer, R. S.: Fog measurements at the site “Falda Verde” north of Chañaral compared with other fog stations of Chile, *Atmos. Res.*, 64, 273–284, [https://doi.org/10.1016/S0169-8095\(02\)00098-4](https://doi.org/10.1016/S0169-8095(02)00098-4), 2002.

Lobos-Roco, F., Suárez, F., Aguirre-Correa, F., Keim, K., Aguirre, I., Vargas, C., Abarca, F., Ramírez, C., Escobar, R., Osses, P., and del Río, C.: Understanding inland fog and dew dynamics for assessing potential non-rainfall water use in the 555 Atacama, *J. Arid Environ.*, 221, <https://doi.org/10.1016/j.jaridenv.2024.105125>, 2024.

Maksaev, V. and Zentilli, M.: Chilean Strata-bound Cu- (Ag) deposits: an overview, in: *Hydrothermal Iron Oxide Copper-*



Gold & Related Deposits: A Global Perspective, edited by: Porter, T. M., PGC Publishing, Adelaide, Australia, 185–205,

2002.

Maksaev, V., Munizaga, F., Fanning, M., Palacios, C., and Tapia, J.: SHRIMP U-Pb dating of the Antucoya porphyry copper deposit: New evidence for an Early Cretaceous porphyry-related metallogenic epoch in the Coastal Cordillera of northern Chile, *Miner. Depos.*, 41, 637–644, <https://doi.org/10.1007/s00126-006-0091-5>, 2006.

560 Marsh, T. M., Einaudi, M. T., and Mcwilliams, M.: 40Ar/ 39Ar geochronology of Cu-Au and Au-Ag mineralization in the Potrerillos District, Chile, *Econ. Geol.*, 92, 784–806, <https://doi.org/10.2113/gsecongeo.92.7-8.784>, 1997.

Martinod, J., Regard, V., Riquelme, R., Aguilar, G., Guillaume, B., Carretier, S., Cortés-Aranda, J., Leanni, L., and Hérail, G.: Pleistocene uplift, climate and morphological segmentation of the Northern Chile coasts (24°S–32°S): Insights from cosmogenic 10Be dating of paleoshorelines, *Geomorphology*, 274, 78–91, <https://doi.org/10.1016/j.geomorph.2016.09.010>, 2016.

565 Mateo, L., Tornos, F., Hanchar, J. M., Villa, I. M., Stein, H. J., and Delgado, A.: The Montecristo mining district, northern Chile: the relationship between vein-like magnetite-(apatite) and iron oxide-copper–gold deposits, *Miner. Depos.*, 58, 1023–1049, <https://doi.org/10.1007/s00126-023-01172-0>, 2023.

Morales-Leal, J. E., Campos, E., Kouzmanov, K., and Riquelme, R.: Alunite supergroup minerals from advanced argillic alteration assemblage in the southern Atacama Desert as indicators of paleo-hydrothermal and supergene environments, *Miner. Depos.*, 58, 593–615, <https://doi.org/10.1007/s00126-022-01149-5>, 2023.

Moreton, S.: Copper-bearing silica gel from the walls of Tankardstown mine, Co. Waterford, Ireland, *J. Russell Soc.*, 10, 10–17, 2007.

575 Mote, T. I., Becker, T. A., Renne, P., and Brimhall, G. H.: Chronology of exotic mineralization at El Salvador, Chile, by 40Ar/ 39Ar dating of copper wad and supergene alunite, *Econ. Geol.*, 96, 351–366, <https://doi.org/10.2113/gsecongeo.96.2.351>, 2001.

Muñoz-Schick, M., Pinto, R., Mesa, A., and Moreira-Muñoz, A.: Fog oases during the El Niño Southern Oscillation 1997–1998, in the coastal hills south of Iquique, Tarapacá region, Chile, 2001.

Murray, R. C.: Origin and Diagenesis of Gypsum and Anhydrite, *SEPM J. Sediment. Res.*, 34, 512–523, <https://doi.org/10.1306/74d710d2-2b21-11d7-8648000102c1865d>, 1964.

Newberg, D. W.: Geochemical implications of chrysocolla-bearing alluvial gravels, *Econ. Geol.*, 62, 932–956, <https://doi.org/10.1080/00206816909475091>, 1967.

585 Oliveros, V., Vásquez, P., Creixell, C., Lucassen, F., Ducea, M. N., Ciocca, I., González, J., Espinoza, M., Salazar, E., Coloma, F., and Kasemann, S. A.: Lithospheric evolution of the Pre- and Early Andean convergent margin, Chile, *Gondwana Res.*, 80, 202–227, <https://doi.org/10.1016/j.gr.2019.11.002>, 2020.

Palacios, C., Ramírez, L. E., Townley, B., Solari, M., and Guerra, N.: The role of the Antofagasta-Calama Lineament in ore deposit deformation in the Andes of northern Chile, *Miner. Depos.*, 42, 301–308, <https://doi.org/10.1007/s00126-006-0113-3>, 2007.



Perelló, J., Martini, R., Arcos, R., and Muhr, R.: Buey Muerto : Porphyry Copper Mineralization in the Early Cretaceous Arc of Northern Chile, 10° Congr. geológico Chil., 1, 2003.

Perelló, J., Muhr, R., Mora, R., Martínez, E., Brockway, H., Swaneck, T., Artal, J., Mpodozis, C., Münchmeyer, C., Clifford, J., Acuña, E., Valenzuela, D., and Argandoña, R.: Wealth Creation through Exploration in a Mature Terrain: The Case 595 History of the Centinela District, Northern Chile Porphyry Copper Belt, in: The Challenge of Finding New Mineral Resources: Global Metallogeny, Innovative Exploration, and New Discoveries, edited by: R. J. Goldfarb, E. E. Marsh, T. Monecke, Society of Economic Geologists, Littleton, U. S. A., 229–252, <https://doi.org/10.5382/SP.15.2>, 2010.

Placzek, C. J., Matmon, A., Granger, D. E., Quade, J., and Niedermann, S.: Evidence for active landscape evolution in the hyperarid Atacama from multiple terrestrial cosmogenic nuclides, *Earth Planet. Sci. Lett.*, 295, 12–20, 600 <https://doi.org/10.1016/j.epsl.2010.03.006>, 2010.

De Putter, T., Mees, F., Decrée, S., and Dewaele, S.: Malachite, an indicator of major Pliocene Cu remobilization in a karstic environment (Katanga, Democratic Republic of Congo), *Ore Geol. Rev.*, 38, 90–100, <https://doi.org/10.1016/j.oregeorev.2010.07.001>, 2010.

Quezada, J., Cerdá, J. L., and Jensen, A.: Efectos de la tectónica y el clima en la configuración morfológica del relieve 605 costero del norte de Chile, *Andean Geol.*, 37, 78–109, <https://doi.org/10.5027/andgeov37n1-a04>, 2010.

Rech, J. A., Quade, J., and Hart, W. S.: Isotopic evidence for the source of Ca and S in soil gypsum, anhydrite and calcite in the Atacama Desert, Chile, *Geochim. Cosmochim. Acta*, 67, 575–586, [https://doi.org/10.1016/S0016-7037\(02\)01175-4](https://doi.org/10.1016/S0016-7037(02)01175-4), 2003.

Reich, M., Palacios, C., Parada, M. A., Fehn, U., Cameron, E. M., Leybourne, M. I., and Zúñiga, A.: Atacamite formation by 610 deep saline waters in copper deposits from the Atacama Desert, Chile: Evidence from fluid inclusions, groundwater geochemistry, TEM, and 36Cl data, *Miner. Depos.*, 43, 663–675, <https://doi.org/10.1007/s00126-008-0184-4>, 2008.

Reich, M., Palacios, C., Vargas, G., Luo, S., Cameron, E. M., Leybourne, M. I., Parada, M. A., Zúñiga, A., and You, C.-F.: Supergene enrichment of copper deposits since the onset of modern hyperaridity in the Atacama Desert, Chile, *Miner. Depos.*, 44, 497–504, <https://doi.org/10.1007/s00126-009-0229-3>, 2009.

615 del Río, C., García, J. L., Osse, P., Zanetta, N., Lambert, F., Rivera, D., Siegmund, A., Wolf, N., Cereceda, P., Larraín, H., and Lobos, F.: ENSO Influence on Coastal Fog-Water Yield in the Atacama Desert, Chile, *Aerosol Air Qual. Res.*, 18, 127–144, <https://doi.org/10.4209/aaqr.2017.01.0022>, 2018.

Riquelme, R., Tapia, M., Campos, E., Mpodozis, C., Carretier, S., González, R., Muñoz, S., Fernández-Mort, A., Sanchez, C., and Marquardt, C.: Supergene and exotic Cu mineralization occur during periods of landscape stability in the Centinela 620 Mining District, Atacama Desert, *Basin Res.*, 30, 395–425, <https://doi.org/10.1111/bre.12258>, 2018.

Ritter, B., Binnie, S. A., Stuart, F. M., Wennrich, V., and Dunai, T. J.: Evidence for multiple Plio-Pleistocene lake episodes in the hyperarid Atacama Desert, *Quat. Geochronol.*, 44, 1–12, <https://doi.org/10.1016/j.quageo.2017.11.002>, 2018a.

Ritter, B., Stuart, F. M., Binnie, S. A., Gerdes, A., Wennrich, V., and Dunai, T. J.: Neogene fluvial landscape evolution in the hyperarid core of the Atacama Desert, *Sci. Rep.*, 8, 1–16, <https://doi.org/10.1038/s41598-018-32339-9>, 2018b.



625 Sato, T.: Manto Type Copper Deposit in Chile-a Review, *Bull. Geol. Surv.*, 35, 565–582, 1984.

Scheuber, E. and González, G.: Tectonics of the Jurassic-Early Cretaceous magmatic arc of the north Chilean Coastal Cordillera (22°-26°S): A story of crustal deformation along a convergent plate boundary, *Tectonics*, 18, 895–910, <https://doi.org/10.1029/1999TC900024>, 1999.

Scheuber, E., Bogdanic, T., Jensen, A., and Reutter, K.-J.: Tectonic Development of the North Chilean Andes in Relation to 630 Plate Convergence and Magmatism Since the Jurassic, *Tectonics South. Cent. Andes*, 121–139, https://doi.org/10.1007/978-3-642-77353-2_9, 1994.

Schwartz, G. M.: Paragenesis of the oxidized ores of copper, *Econ. Geol.*, 29, 55–75, <https://doi.org/https://doi.org/10.2113/gsecongeo.29.1.55>, 1934.

Schween, J. H., Del Rio, C., García, J. L., Osses, P., Westbrook, S., and Löhnert, U.: Life cycle of stratocumulus clouds over 635 1 year at the coast of the Atacama Desert, *Atmos. Chem. Phys.*, 22, 12241–12267, <https://doi.org/10.5194/acp-22-12241-2022>, 2022.

Sillitoe, R. H.: Supergene Oxidized and Enriched Porphyry Copper and Related Deposits, in: One Hundredth Anniversary Volume, 723–768, <https://doi.org/https://doi.org/10.5382/AV100.22>, 2005.

Sillitoe, R. H. and McKee, E. H.: Age of Supergene Oxidation and Enrichment in the Chilean Porphyry Copper Province., 640 *Econ. Geol.*, 91, 164–179, <https://doi.org/https://doi.org/10.2113/gsecongeo.91.1.164>, 1996.

Sofer, Z.: Isotopic composition of hydration water in gypsum, *Geochim. Cosmochim. Acta*, 42, 1141–1149, [https://doi.org/10.1016/0016-7037\(78\)90109-6](https://doi.org/10.1016/0016-7037(78)90109-6), 1978.

Throop, A. H. and Buseck, P. R.: Nature and Origin of Black Chrysocolla at the Inspiration Mine, Arizona, *Econ. Geol.*, 66, 1168–1175, <https://doi.org/https://doi.org/10.2113/gsecongeo.66.8.1168>, 1971.

645 Torpy, A., Fan, R., Wilson, N., MacRae, C., and Austin, P.: Quantifying Trace Element Variations in Chrysocolla by Clustering FEG-EPMA Hyperspectral Maps, *Microsc. Microanal.*, 27, 1870–1872, <https://doi.org/10.1017/s1431927621006826>, 2021.

Tristá-Aguilera, D., Barra, F., Ruiz, J., Morata, D., Talavera-Mendoza, O., Kojima, S., and Ferraris, F.: Re-Os isotope systematics for the Lince-Estefanía deposit: Constraints on the timing and source of copper mineralization in a stratabound 650 copper deposit, Coastal Cordillera of Northern Chile, *Miner. Depos.*, 41, 99–105, <https://doi.org/10.1007/s00126-006-0048-8>, 2006.

Trista, D. and Kojima, S.: Mineral paragenesis and fluid inclusions of some pluton-hosted vein-type copper deposits in the Coastal Cordillera, northern Chile, *Resour. Geol.*, 53, 21–28, <https://doi.org/10.1111/j.1751-3928.2003.tb00154.x>, 2003.

Vivallo, W. and Henríquez, F.: Génesis común de los yacimientos estratoligados y vetiformes de cobre del Jurásico Medio a 655 Superior en la Cordillera de la Costa, Región de Antofagasta, Chile., *Rev. Geológica Chile*, 25, 199–228, 1998.

Warren, I., Archibald, D. A., and Simmons, S. F.: Geochronology of epithermal Au-Ag mineralization, magmatic-hydrothermal alteration, and supergene weathering in the El Peñón district, Northern Chile, *Econ. Geol.*, 103, 851–864, <https://doi.org/https://doi.org/10.2113/gsecongeo.103.4.851>, 2008.



Yates, D. M., Joyce, K. J., and Heaney, P. J.: Complexation of copper with polymeric silica in aqueous solution, Appl. 660 Geochemistry, 13, 235–241, [https://doi.org/10.1016/S0883-2927\(97\)00062-0](https://doi.org/10.1016/S0883-2927(97)00062-0), 1998.